The protocol for the microwell version of the mouse lymphoma assay was described by Chen and Moore [2004]. 3′-Azido-3′-deoxythymidine (AZT) was obtained from Cipla (Mumbai, India), through its U.S. supplier (Bryon Chemical, Long Island City, NY), and dimethylsulfoxide (DMSO) and trifluorothymidine (TFT) were obtained from Sigma (St. Louis, MO). Briefly, cells were centrifuged and resuspended at a concentration of 0.2 $\times$ 10^6 cells/ml in 50 ml of medium in 75-cm^2 polystyrene flasks. AZT was dissolved in DMSO. Different concentrations of AZT were added to the cell cultures in a final volume of 200 μl (control cells were exposed to 200 μl DMSO), and the final concentrations of AZT ranged from 100 to 1,000 μg/ml (374–3,742 μM). The flasks were incubated at 37°C in an atmosphere of 5% CO_2 with saturated humidity for 24 hr. The cells were then centrifuged, washed with fresh medium twice, and resuspended in fresh medium. The cells were transferred to new 75-cm^2 flasks and maintained in logarithmic growth for a 2-day expression period. Then the cells were cloned in 96-well plates in medium containing 3 μg/ml TFT for selection and medium without TFT for the measurement of cloning efficiency. All plates were incubated in an atmosphere of 5% CO_2 with saturated humidity at 37°C for 12 days. The colonies were counted and the colony-size was determined by eye using a Quebec dark field colony counter. Total, small colony (SC), and large colony (LC) *Tk* MFs were determined and the relative total growth (RTG) value that measures cytotoxicity was calculated according to the published protocol [Chen and Moore, 2004].

Tk Mutant Isolation and DNA Extraction

One hundred and fifty mutants were randomly selected and isolated from the culture treated with the highest test dose of AZT (1 mg/ml, 3,742 μM). Sixty nine spontaneous mutants were isolated from independent untreated cultures over a period of approximately 2 months (one large and one small colony mutant were randomly isolated from each independent culture). All of the isolated mutant colonies were grown in medium containing 3 μg/ml TFT to confirm their phenotype.

Genomic DNA was extracted from 3 $\times$ 10^6 cells of each *Tk* mutant clone using the Qiagen DNeasy tissue kit (Valencia, CA; protocol version: March 2004) and stored at −20°C.

Tk Gene LOH Analysis

Tk gene LOH analysis was conducted using the microsatellite PCR described by Liechty et al. [1996], with some modifications. Briefly, the microsatellite locus *D11Agl2* that resides in the *Tk* gene was amplified using primers Agl2.frw and Agl2.rev [Liechty et al., 1996]. PCR amplifications were conducted in a total volume of 20μl: 2 μl of the extracted mutant DNA were mixed with 10 μl PCR Master Mix (Promega, Madison, WI), primers, and water. The final amount of each reagent was: 1× Taq polymerase reaction buffer, 10 pmol of each primer, 12.5 nmol of each dNTP, and 0.25 U Taq DNA polymerase. The PCR was performed in 96-well plates using a PCR System 9700 (Applied Biosystems, Foster City, CA), with the following touch-down method: a 3 min denaturation at 95°C; followed by 2 cycles of 30 sec denaturation at 95°C, 30 sec annealing at 72°C, and 30 sec extension at 72°C. The annealing temperature was then decreased by 1°C for each additional two cycles until 65°C was reached. Then 20 additional cycles were performed at the 65°C annealing temperature, followed by a final extension at 72°C for 7 min. The reaction products were separated by 2% agarose gel electrophoresis, stained with 1 μg/ml ethidium bromide, and visualized with a UV transilluminator.

Chromosome 11 LOH Analysis

In addition to microsatellite marker *D11Agl2*, 8 other informative microsatellite loci on mouse chromosome 11 (*D11Mit 42, 59, 36, 29, 22, 20, 19,* and *74*) were identified from the mouse genome data base (Jackson Laboratory, Bar Harbor, ME, http://www.informatics.jax.org). The 9 microsatellite loci are almost evenly distributed along the length of the chromosome (with locations at 78.0, 72.0, 58.5, 47.6, 40.0, 25.0, 20.0, 13.0, and 0.0 cM, respectively). LOH analysis was performed at each microsatellite locus using allele-specific PCR.

The same PCR amplification conditions were used for the 8 loci. The conditions varied from those used for *D11Agl2* in the cycling parameters: a 5 min denaturation at 95°C; followed by 40 cycles of 30 sec denaturation at 95°C, 30 sec annealing at 59°C, and 45 sec extension at 72°C; and a final extension of 10 min at 72°C. The reaction products were separated and visualized as above.

Tk Gene-Dosage Analysis

For those mutants showing LOH at the *Tk* locus, *Tk* gene copy number (CN) was further evaluated using a Real-Time PCR method. A 170-base DNA fragment in intron 2 of the *Tk* gene and a 192-base fragment in exon 3 of an unrelated reference gene (*H-2K*) on chromosome 17 were amplified separately and simultaneously [Honma et al., 2001]. The fragment in the *H-2K* gene was used as an endogenous reference for PCR quantification based on the fact that the amplification efficiencies are approximately equal for the *H-2K* and *Tk* fragments (the absolute value of the slope of the relative efficiency plot for the two amplification reactions, <0.1).

The PCR conditions for the two fragments were the same. Real-Time PCR amplification was conducted in a total volume of 50 μl; 2 μl of the extracted mutant DNA was mixed with 25 μl iQ SYBR Green Supermix (Bio-Rad, Hercules, CA), primers, and water. The final amount of each reagent was: 1× Taq polymerase reaction buffer, 20 pmol of each primer, 10 nmol of each dNTP, 1.25 U iTaq DNA polymerase, and 0.5 pmol SYBR green fluorescein. The PCR reaction was performed in 96-well plates using an iCycler iQ Real-Time PCR detection system (Bio-Rad), with the following cycling parameters: a 5 min denaturation at 95°C; followed by 40 cycles of 30 sec denaturation at 95°C, 30 sec annealing at 59°C, and 30 sec extension at 72°C; and a final extension of 10 min at 72°C.

When the amount of amplification product reached a given threshold in the exponential phase, the cycle number of the two amplification reactions was measured using the iCycler iQ optical system software (version 3.0a, Bio-Rad). Each quantitative PCR reaction was repeated three times and the mean cycle number was used for the calculation. The *Tk* gene CN for each of the mutants was calculated as follows:

1. Because the amplification efficiencies were almost the same for the two PCR reactions, the relative cycle number of wild-type *Tk* amplification ($C_{W\text{-}Tk\text{-}Relative}$) was adjusted by the *H-2K* amplification (comparative ΔC_T method):

$$C_{W\text{-}Tk\text{-}Relative} = C_{W\text{-}Tk} + (C_{M\text{-}H2K} - C_{W\text{-}H2K})$$

[$C_{W\text{-}Tk}$ is the cycle number of *Tk* gene amplification using DNA isolated from wild-type ($Tk^{+/-}$) mouse lymphoma cells; $C_{M\text{-}H2K}$ is the cycle number of *H-2K* gene amplification using DNA isolated from the *Tk* mutant; $C_{W\text{-}H2K}$ is the cycle number of *H-2K* gene amplification using DNA isolated from wild-type ($Tk^{+/-}$) mouse lymphoma cells.]

2. The cycle number difference (CD) of the *Tk* gene amplification between the *Tk* mutant and wild-type ($Tk^{+/-}$) cells was calculated as:

$$CD = C_{M\text{-}Tk} - C_{W\text{-}Tk\text{-}Relative}$$

($C_{M\text{-}Tk}$ is the cycle number of *Tk* gene amplification using DNA isolated from the *Tk* mutant.)

3. The *Tk* gene CN of each mutant was then calculated based on the fact that $Tk^{+/-}$ cells have two copies of the *Tk* gene.

$$CN = 2^{1-CD}$$

For example, if CD = 1, then CN = 1: the *Tk* gene was hemizygous (1 copy); if CD = 0, then CN = 2: there were 2 copies of the *Tk* gene.

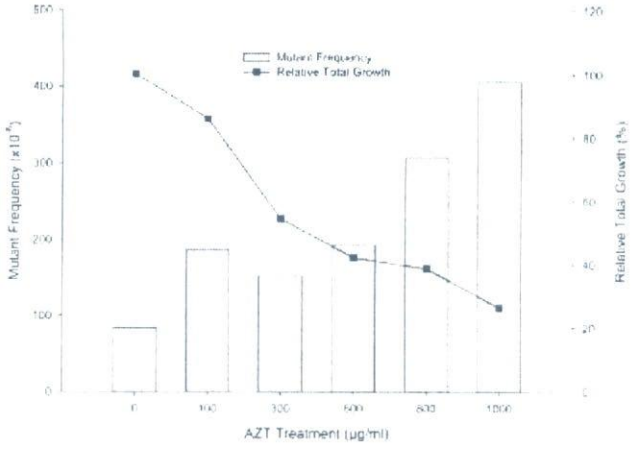

Fig. 1. Tk mutant frequency and relative total growth of L5178Y/$Tk^{+/-}$ mouse lymphoma cells treated with AZT. The doses in molarity are 0, 374, 1,123, 2,245, 2,994, and 3,742 μM, respectively.

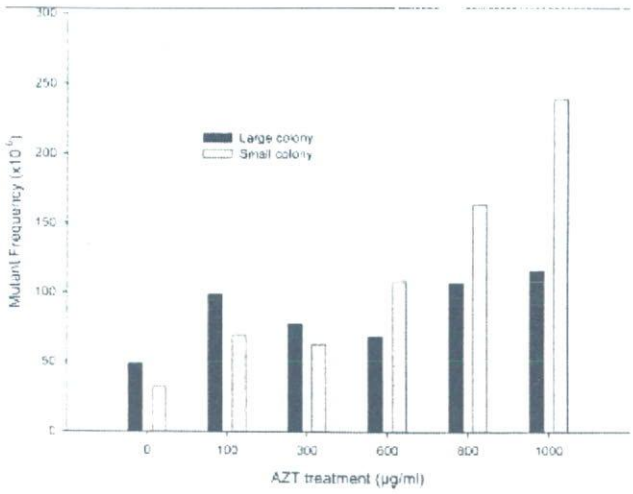

Fig. 2. Large and small colony *Tk* mutant frequencies of L5178Y/$Tk^{+/-}$ mouse lymphoma cells treated with AZT. The doses in molarity are 0, 374, 1,123, 2,245, 2,994, and 3,742 μM, respectively.

According to the criteria set by Honma et al. [2001], the CN of *Tk* mutants was classified as <1.2, 1.2–1.8, and >1.8, which sets the ranges for the hemizygous, mosaic, and homozygous states of the *Tk* gene, respectively [Honma et al., 2001].

Statistical Analysis

The computer program written by Cariello [1994] for the Monte Carlo analysis developed by Adams and Skopek [1987] was used to compare the chromosome 11 LOH patterns and mutation spectra between different groups of mutants.

Weighted sums of the number of LC and SC mutants were used in the comparison of LOH patterns and mutation spectra between different groups considering the proportion difference of LC and SC mutants between the selected mutants and mutants in the original culture (the proportion of SC mutants was 65 and 40% in the AZT-treated culture and control, respectively).

For each class of mutants, the total number including both LC and SC mutants was calculated as the weighted sum of the number of LC and SC mutants:

1. For the mutants from the AZT-treated culture

$$\text{Weighted sum} = 150 \times (35\% \times \text{Number of LC mutants}/55 + 65\% \times \text{Number of SC mutants}/95)$$

2. For the spontaneous mutants

$$\text{Weighted sum} = 69 \times (60\% \times \text{Number of LC mutants}/36 + 40\% \times \text{Number of SC mutants}/33)$$

RESULTS

Tk Mutation Assay

AZT induced dose-related cytotoxicity and mutagenicity responses in L5178Y/$Tk^{+/-}$ mouse lymphoma cells (Fig. 1). AZT (0.8 and 1 mg/ml) (2,994 and 3,742 μM) produced clear increases in *Tk* MF over that of the vehicle control. The results were evaluated using the new criteria developed by the Mouse Lymphoma Expert Working Group of the International Workshop for Genotoxicity Testing (IWGT) [Moore et al., 2006]. For a response to be positive for the microwell version of the assay, these guidelines require an induced MF of at least 126×10^{-6} [the Global Evaluation Factor (GEF)] in one or more treated cultures while showing cytotoxicity ≥10% RTG. A positive dose response must also be observed. AZT induced more small colony mutants than large colony mutants (Fig. 2).

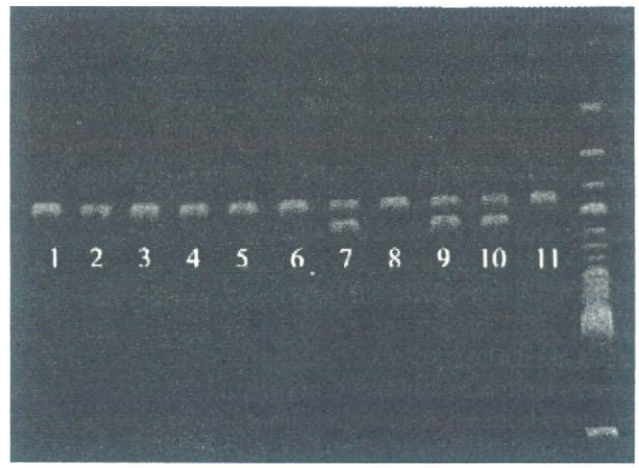

Fig. 3. PCR analysis of the loss of heterozygosity (LOH) at the D11Agl2 microsatellite locus that resides in the *Tk* gene of L5178Y mouse lymphoma cells. Note that mutants 1–6, 8 and 11 show LOH (the 523 bp product is lost).

LOH Analysis

Nine polymorphic microsatellite markers (*D11Agl2*, and *D11Mit 42, 59, 36, 29, 22, 20, 19*, and *74*) that were almost evenly distributed along the full length of chromosome 11

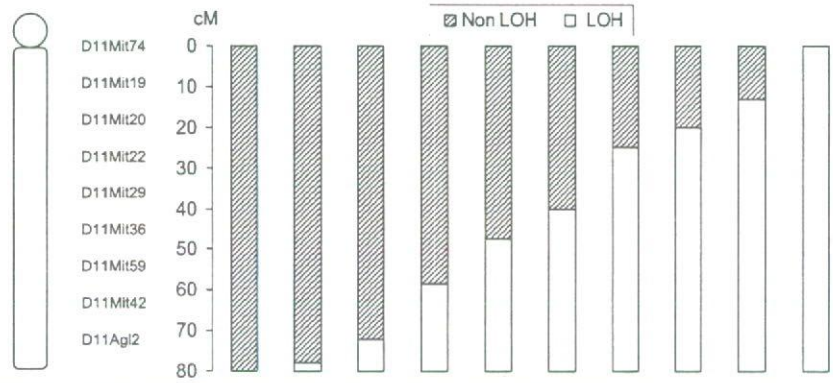

	Microsatellites	R	Mutants showing LOH that extends to									D-LOH
			Agl2	*42*	*59*	*36*	*29*	*22*	*20*	*19*	*74*	
Mutants from AZT-treated culture*	LC (55)	14	6	10	4	6	4	1	0	3	7	0
		25%	11%	18%	7%	11%	7%	2%	0%	5%	13%	0%
	SC (95)	0	7	38	8	9	6	1	3	6	14	3
		0%	7%	40%	8%	9%	6%	1%	3%	6%	15%	3%
	Total** (150)	13	13	49	12	15	10	2	3	9	21	3
		9%	9%	33%	8%	10%	7%	1%	2%	6%	14%	2%
Spontaneous mutants	LC (36)	21	3	1	0	2	2	2	0	0	5	0
		58%	8%	3%	0%	6%	6%	6%	0%	0%	14%	0%
	SC (33)	1	3	11	2	0	3	0	3	1	9	0
		3%	9%	33%	6%	0%	9%	0%	9%	3%	27%	0%
	Total** (69)	25	6	10	2	2	5	2	3	1	13	0
		36%	9%	14%	3%	3%	7%	3%	4%	1%	19%	0%

Fig. 4. Loss of heterozygosity (LOH) analysis of chromosome 11 in mouse lymphoma *Tk* mutants from the AZT-treated culture and untreated independent control cultures (LC: large colony; SC: small colony; R: retain heterozygosity; D-LOH: discontinuous LOH).*The culture that the analyzed mutants were isolated from was treated with 1 mg/ml (3,742 μM) AZT for 24 hr.**Total is the weighted sum of the number of LC and SC mutants considering the proportion difference of LC and SC mutants between the selected mutants and mutants in the original culture (the proportion of SC mutants was 65 and 40% in the AZT-treated culture and control, respectively). The discontinuous LOH patterns of three SC mutants from the AZT-treated culture are shown in Table I.

were identified and used to investigate the extent of chromosome 11 LOH. One hundred and fifty mutants (55 LC and 95 SC mutants) from the 1 mg/ml (3,742 μM) AZT-treated culture and sixty-nine independent spontaneous mutants (36 LC and 33 SC mutants) were analyzed (Figs. 3 and 4). All (95 of 95) of the SC mutants from the AZT-treated culture showed LOH at the *Tk* gene. All but one (32 of 33) of the SC mutants from the untreated control cultures also showed LOH at the *Tk* gene. The primary difference in *Tk* LOH between the mutants from untreated and AZT-treated cultures occurred with the LC mutants. *Tk* LOH was observed in 41 of 55 LC mutants (75%) from the AZT-treated culture but in only 15 of 36 LC mutants (42%) from the untreated control. In total, 91% of the mutants from the AZT-treated culture had LOH at the *Tk* locus while 64% of the spontaneous mutants had *Tk* LOH.

Figure 4 shows the number of mutants having each of the various LOH patterns. For instance, 10 LC mutants from the AZT-treated culture had LOH at both the *Tk* and Mit42 loci. These 10 mutants were heterozygous at all of the rest of the 7 microsatellite markers. Only three SC mutants (all from the AZT-treated culture) showed discontinuous LOH patterns (Table I).

TABLE I. Discontinuous Loss of Heterozygosity (LOH) Patterns of Chromosome 11 in Three Mouse Lymphoma *Tk* Mutants from the AZT-Treated Culture[a]

	Microsatellites								
	Agl2	*42*	*59*	*36*	*29*	*22*	*20*	*19*	*74*
Mutant 1	○	○	○	○	●	○	○	●	●
Mutant 2	○	○	●	●	●	●	●	●	○
Mutant 3	○	○	●	●	○	●	●	●	●

(●: retain heterozygosity; ○: LOH).

[a]The culture that these three mutants were isolated from was treated with 1 mg/ml (3,742 μM) AZT for 24 hr. Microsatellite marker D11Agl2 was identified by Liechty et al. [1996]; all the other markers were selected from the mouse genome data base (Jackson Laboratory, Bar Harbor, ME, http://www.informatics.jax.org).

The LOH patterns of mutants from the AZT-treated culture were significantly different from those of spontaneous mutants isolated from independent cultures ($P < 0.01$). This difference was primarily due to the difference between the LC mutants from the AZT-treated culture and the spontaneous LC mutants ($P < 0.01$). The SC mutants from the AZT-treated culture and spontaneous SC mutants did not show significant difference in their LOH patterns ($P >$

TABLE II. *Tk* Gene Copy Number of Mouse Lymphoma Mutants from the AZT-Treated Culture and Independent Untreated Control Cultures. Data are Presented to Show Both *Tk* Gene Copy Number and the Extent of Chromosomal LOH as Measured by Microsatellite Analysis

Source of mutants	Clone size (No.)	CN of *Tk* gene	LOH extends to									
			Agl2	*42*	*59*	*36*	*29*	*22*	*20*	*19*	*74*	D
Mutants from AZT-treated culture[a]	LC (55)	<1.2	4	1	1	2	3			1	1	
		1.2–1.8	1	3	1	1						
		>1.8	1	6	2	3	1	1		2	6	
	SC (95)	<1.2	5	23	3	4	1	1		1	2	
		1.2–1.8		6	1	2	1				2	
		>1.8	2	9	4	3	4		3	5	10	3
Spontaneous mutants	LC (36)	<1.2										
		1.2–1.8	1									
		>1.8	2	1		2	2	2			5	
	SC (33)	<1.2	1	5			3				1	
		1.2–1.8	2	3							1	
		>1.8		3	2				3	1	7	

CN: copy number; LOH: loss of heterozygosity; LC: large colony; SC: small colony; D: discontinuous LOH.

[a]The culture that the analyzed mutants were isolated from was treated with 1 mg/ml (3,742 μM) AZT for 24 hr. Microsatellite marker *D11Agl2* was identified by Liechty et al. [1996]; all the other markers were selected from the mouse genome data base (Jackson Laboratory, Bar Harbor, ME, http://www.informatics.jax.org).

0.05). In addition, the LOH patterns of LC and SC mutants were distinct from each other, both for the mutants from the AZT-treated culture and the spontaneous mutants ($P < 0.01$).

Tk Gene Dosage Analysis

The CN of the *Tk* gene in mutants showing LOH at the *Tk* gene was measured using a Real-Time PCR method and classified according to the criteria set by Honma et al. [2001]. The hemizygous state of the *Tk* gene (CN < 1.2) indicates a deletion of the Tk^+ allele or a complete chromosome loss; the homozygous state of *Tk* gene (CN > 1.8) indicates that the mutant resulted from recombination or chromosome duplication after chromosome loss. The mutants showing an intermediate CN (1.2–1.8) may be mosaic or the result of complex rearrangements [Honma et al., 2001, 2003].

Table II shows the combined results of the chromosome 11 microsatellite LOH analysis and the *Tk* gene dosage analysis of 150 *Tk* mutants from the 1 mg/ml (3,742 μM) AZT-treated culture and 69 independent mutants from untreated controls. Table III shows the mutation type classification based on the chromosome 11 microsatellite LOH pattern and the *Tk* gene CN, and Table IV shows the summary of the mutation spectra of mutants from the AZT-treated culture and the independent spontaneous mutants. The mutation types are: (1) intragenic mutation (retains heterozygosity at the *Tk* locus; includes point mutation, frame shifts, and small intragenic deletions), (2) deletion (LOH at the *Tk* locus with *Tk* gene CN < 1.2, and retaining heterozygosity of at least one microsatellite marker), (3) chromosome loss (*Tk* gene CN < 1.2, and all microsatellite markers showing LOH), (4) recombination (LOH at the *Tk* locus with *Tk* gene CN > 1.8, and retaining heterozygosity of at least one microsatellite marker), (5) chromosome duplication after chromosome loss (*Tk* gene CN > 1.8, and all markers showing LOH), and (6) other events, including mosaic events or complicated rearrangements (LOH at *Tk* locus with *Tk* gene CN between 1.2 and 1.8).

TABLE III. Classification of Mouse Lymphoma *Tk* Mutants Based on Chromosome 11 Microsatellite LOH Pattern and *Tk* Gene Copy Number

Mutation type	LOH analysis	*Tk* gene copy number
Intragenic mutation	Retain heterozygosity at the *Tk* locus	NA
Deletion	LOH at the *Tk* locus, retain heterozygosity of at least one microsatellite marker	<1.2
Chromosome loss	All markers show LOH	<1.2
Recombination	LOH at the *Tk* locus, retain heterozygosity of at least one microsatellite marker	>1.8
Chromosome duplication	All markers show LOH	>1.8
Mosaic/Complex	LOH at the *Tk* locus	1.2–1.8

NA: Not analyzed.

The mutation spectrum of mutants from the AZT-treated culture was significantly different from the spectrum of independent spontaneous mutants ($P < 0.01$). A lower proportion of intragenic mutations and a higher proportion of deletions were observed in the mutants from the AZT-treated culture. The difference in the mutation spectrum between the spontaneous mutants and mutants from the AZT-treated culture was primarily due to a difference between the LC mutants ($P < 0.01$). The SC mutants did not show any significant difference in their mutation spectrum ($P > 0.05$). In addition, the LC and SC mutants had distinct mutation spectra, both for the mutants from the AZT-treated culture and for the untreated control ($P < 0.01$).

TABLE IV. Mutation Spectra of Mouse Lymphoma *Tk* Mutants from the AZT-Treated Culture and Untreated Independent Control Cultures

Source of mutants	Clone size (No.)	Intragenic mutation	Deletion	Chromosome loss	Recombination	Chromosome duplication	Mosaic/ Complex
Mutants from AZT-treated culture[a]	LC (55)	14 (25%)	12 (22%)	1 (2%)	16 (29%)	6 (11%)	6 (11%)
	SC (95)	0 (0%)	39 (41%)	2 (2%)	32 (34%)	10 (11%)	12 (13%)
	Total[b] (150)	13 (9%)	51 (34%)	3 (2%)	48 (32%)	16 (11%)	18 (12%)
Spontaneous mutants	LC (36)	21 (58%)	0 (0%)	0 (0%)	9 (25%)	5 (14%)	1 (3%)
	SC (33)	1 (3%)	9 (27%)	1 (3%)	9 (27%)	7 (21%)	6 (18%)
	Total[b] (69)	25 (36%)	8 (11%)	1 (1%)	18 (26%)	12 (17%)	6 (9%)

LC: large colony; SC: small colony.

[a]The culture that the analyzed mutants were isolated from was treated with 1 mg/ml (3,742 μM) AZT for 24 hr.

[b]Total is the weighted sum of the number of LC and SC mutants considering the proportion difference of LC and SC mutants between the selected mutants and mutants in the original culture (the proportion of SC mutants was 65 and 40% in the AZT-treated culture and untreated control, respectively).

The SC mutants contained more deletions and fewer intragenic mutations than did the LC mutants.

DISCUSSION

AZT, a synthetic thymidine analogue developed to treat AIDS, has been used widely to treat and prevent HIV infection since its approval by the US FDA in 1987. Its therapeutic effect is due to the inhibition of HIV reverse transcriptase as well as the termination of proviral DNA synthesis. However, AZT also can incorporate into the mammalian cell nuclear DNA and the incorporation is closely correlated with its genotoxicity [Vazquez-Padua et al., 1990; Sussman et al., 1999; Meng et al., 2000b]. Molecular analysis indicates that the majority of AZT-induced mutations in autosomal genes are due to LOH [Meng et al., 2000a,b; Von Tungeln et al., 2002]. LOH is an important mechanism for the functional loss of critical genes, such as tumor suppressor genes, and it is the most common mutational mechanism in the etiology of human cancer [Lasko and Cavenee, 1991; Wijnhoven et al., 2001; Thiagalingam et al., 2002]. Our data are consistent with those previous findings. At a dose of 1 mg/ml (3,742 μM), 91% of AZT-induced mutants showed LOH at the *Tk* locus while *Tk* LOH was detected in only 64% of spontaneous mutants.

AZT is a thymidine analogue; therefore, using the *Tk* gene as the mutational target raises the issue that the increase in MF might be due to selection of pre-existing mutants rather than induction of new mutants. AZT is activated by a series of phosphorylation reactions to AZT triphosphate to elicit its therapeutic effects as well as its toxicity. The first step of the activation (AZT → AZT monophosphate) is catalyzed by thymidine kinase [Veal and Back, 1995]. Because AZT cannot be activated without a functional Tk, this raises the possibility that the pre-existing $Tk^{-/-}$ mutants may avoid the toxicity of AZT. As a consequence, the pre-existing mutants may gain a growth advantage over the $Tk^{+/-}$ cells and the *Tk* MF will be increased by this differential cytotoxicity. In studies using B6C3F1/$Tk^{+/-}$ mice, Von Tungeln et al. [2002] and Mittelstaedt et al. [2004] found that the percentage of mutants showing LOH at the *Tk* locus and also the LOH pattern differed between the mutants from the AZT-treated animals and the untreated control animals. Their results indicated that de novo mutation induction rather than pre-existing mutant selection played the major role in the MF elevation. Our study, by further clarifying the AZT-induced mutation spectrum in mouse lymphoma cells, confirms this conclusion. The mutation spectrum of mutants from the AZT-treated culture was distinct from that of the spontaneous mutants. If the MF increase was primarily due to mutant selection, then the mutation spectra of mutants from AZT-treated culture and untreated control should have been the same.

Mittelstaedt et al. [2004] found a relatively high proportion of discontinuous LOH patterns in the mutants from AZT-treated B6C3F1/$Tk^{+/-}$ mice. Von Tungeln et al. [2007] also found discontinuous LOH patterns in the mutants from neonatal offspring of B6C3F1/$Tk^{+/-}$ mice transplacetally exposed to AZT. Discontinuous LOH is two areas of LOH in a single chromosome interrupted by a section of the chromosome without LOH. *Tk* mutant lymphocytes (20%) isolated from the AZT-treated mice contained discontinuous LOH and no discontinuous LOH was observed in the control [Mittelstaedt et al., 2004]. Discontinuous LOH is thought to result from chromosome instability and it is caused by multiple deletions and/or mitotic recombination events [Turker et al., 1999]. Turker et al. [1999] observed these novel LOH patterns in an *Aprt*$^{+/-}$ kidney cell line after exposure to hydrogen peroxide. They hypothesized that the discontinuous LOH resulted from oxidative damage. Later Ponomareva et al. [2002] observed this pattern in ionizing radiation-induced *Aprt* mutants from ear and kidney tissues and they suspected that it resulted from genomic instability following mutation. In our study, we found only three out of 150 mutants from the AZT-treated culture had discontinuous LOH. The reason for this difference in discontinuous LOH generation in mouse lymphoma cells and the lymphocytes of $Tk^{+/-}$ mice [Mittelstaedt et al., 2004] is not clear.

LOH is thought to result from either a deletion or a recombination event between homologous alleles during the repair of DNA double-strand breaks (DSBs) [Honma, 2005]. Mutation types are determined not only by the nature of the DNA damage but also by the nature of the DNA repair. Different DNA repair pathways may yield different types of mutation [Pastink et al., 2001]. DSBs are usually induced by ionizing radiation, clastogens, and endogenously generated reactive oxygen species. Their repair is important to the maintenance of genomic integrity, which is essential for cellular survival in mammals [Khanna and Jackson, 2001]. In mammalian cells, there are two main pathways for the repair of DNA DSBs: nonhomologous end-joining (NHEJ) and homologous recombination (HR), with NEHJ as the major repair pathway [Jackson, 2002; Helleday, 2003; Honma et al., 2003]. NHEJ repairs DSBs by processing the two broken DNA ends first, followed by joining and ligation. Since this repair mechanism occurs in a nonconservative manner, it often results in deletions. Although HR is conservative and usually error-free, it may result in recessive mutation when the template allele has a mutation. Both NEHJ and HR result in LOH [Rathmell and Chu, 1998]. In addition, there is evidence indicating that illegitimate (nonhomologous) recombination is also an important pathway for DSB repair in mammalian cells and significantly contributes to the generation of LOH in p53-mutant cells [Honma et al., 1997; Sargent et al., 1997]. Because the L5178Y mouse lymphoma cell line has two mutant *p53* alleles [Storer et al., 1997; Clark et al., 1998], this mechanism may contribute to the LOH induced by AZT in these cells.

LOH has been studied in various systems, but very few studies further investigated the nature of the LOH. Most previous studies provided data from which the authors speculated as to the actual mutation events [Turker et al., 1999]. Without gene dosage analysis and cytogenetic analysis, such predictions may not be correct. Southern blot analysis has been used to detect allele polymorphism and gene dosage [Applegate et al., 1990; Clive et al., 1990; Meng et al., 2002]. However, this method has several disadvantages. It is time consuming, requires a relatively large amount of DNA, and cannot measure gene dosage with precision [Joseph et al., 1993]. Cytogenetic analysis of mutants is also informative [Hozier et al., 1981; Moore et al., 1985; Blazak et al., 1989; Zhang et al., 1996]. Wijnhoven et al. [1998] used a dual-colored FISH-analysis to measure the gene dosage in the *Aprt* locus. However, because cytogenetic analysis is also time consuming and technically demanding, the number of mutants that can be reasonably analyzed is somewhat limited. For this study, we developed a Real-Time PCR method to detect *Tk* gene dosage rapidly and with satisfactory precision. We used an unrelated gene (*H-2K*) that resides on chromosome 17 as an endogenous reference [Honma et al., 2001]. In the L5178Y/$Tk^{+/-}$ 3.7.2C mouse lymphoma cell line, chromosome 17 is cytogenetically stable and diploid [Sawyer et al., 2005].

A higher proportion of deletions (34% vs. 11%) and a lower proportion of intragenic mutations (9% vs. 36%) were observed in the mutants from the AZT-treated culture compared with the spontaneous mutants; while the proportion of recombination events increased only slightly in the mutants from the AZT-treated culture compared with the spontaneous mutants (32% vs. 26%). These data indicate that AZT mainly induces large-scale DNA damage in mouse lymphoma cells and a large number of induced mutations are deletions. The greatly increased frequency of deletions may result from insufficient HR repair, NEHJ repair, or illegitimate recombination [Sargent et al., 1997; Honma et al., 2003].

The DSBs induced by AZT are a severe form of DNA damage, and normal cells with unrepaired DSBs usually can not survive. DSBs lead to cell death through *p53*-dependent pathways [Khanna and Jackson, 2001; Honma, 2005]. Honma et al. [2000, 2005] conducted extensive research on the effects of p53 status on mutation manifestation in human lymphoblastoid cell lines and found that a higher frequency of large deletions and chromosome changes were induced in p53-mutant cell lines. Our data are consistent with these findings. In the L5178Y/$Tk^{+/-}$ - 3.7.2C mouse lymphoma cell line, both *p53* alleles are mutant [Storer et al., 1997; Clark et al., 1998], and this may explain why a large number of mutants with large deletions survived.

In summary, the genotoxicity of AZT has been characterized in L5178Y/$Tk^{+/-}$ mouse lymphoma cells. Taking advantage of a Real-Time PCR technique, our study is the first to clarify the mutation spectrum induced by AZT. A large number of the mutants from AZT-treated culture result from deletion.

ACKNOWLEDGMENTS

This research was supported in part by an appointment (J. Wang) to the Research Participation Program at the National Center for Toxicological Research administrated by the Oak Ridge Institute of Science and Education through an interagency agreement between the U.S. Department of Energy and the U.S. Food and Drug Administration. The authors thank Drs. Robert H. Heflich and Nan Mei for their review of this manuscript and their enlightening comments. The views presented in this article do not necessarily reflect those of the U.S. Food and Drug Administration.

REFERENCES

Adams WT, Skopek TR. 1987. Statistical test for the comparison of samples from mutational spectra. J Mol Biol 194:391–396.

Agarwal RP, Olivero OA. 1997. Genotoxicity and mitochondria damage in human lymphocytic cells chronically exposed to 3′-azido-3′-dideoxythymidine. Mutat Res 390:223–231.

Applegate ML, Moore MM, Broder CB, Burrell A, Juhn G, Kasweck KL, Lin PF, Wadhams A, Hozier JC. 1990. Molecular dissection of mutations at the heterozygous thymidine kinase locus in mouse lymphoma cells. Proc Natl Acad Sci USA 87:51–55.

Ayers KM, Clive D, Tucker WE, Hajian G, Miranda PD. 1996. Nonclinical toxicology studies with zidovudine: Genetic toxicity tests and carcinogenicity bioassays in mice and rats. Fundam Appl Toxicol 32:148–158.

Ayers KM, Torrey CE, Reynolds DJ. 1997. A transplacental carcinogenicity bioassay in CD-1 mice with zidovudine. Fundam Appl Toxicol 38:195–198.

Blazak WF, Los FJ, Rudd CJ, Caspary WJ. 1989. Chromosome analysis of small and large L5178Y mouse lymphoma cell colonies: Comparison of trifluorothymidine-resistant and unselected cell colonies from mutagen-treated and control cultures. Mutat Res 224:197–208.

Cariello NF. 1994. Software for the analysis of mutations at the human *Hprt* gene. Mutat Res 312:173–185.

Chen T, Moore MM. 2004.Screening for chemical mutagens using the mouse lymphoma assay. In: Yan Z,Caldwell GW, editors. Optimization in Drug Discovery: In-Vitro Methods. Totowa, NJ: Humana Press. pp 337–352.

Clark LS, Hart DW, Vojta PJ, Harrington-Brock K, Barrett JC, Moore MM, Tindall KR. 1998. Identification and chromosomal assignment of two heterozygous mutations in the *Trp53* gene in L5178Y $Tk^{+/-}$ 3.7.2 C mouse lymphoma cells. Mutagen 13:427–434.

Clive D, Glover P, Applegate M, Hozier J. 1990. Molecular aspects of chemical mutagenesis in L5178Y/$Tk^{+/-}$ mouse lymphoma cells. Mutagen 5:191–197.

Connor EM, Sperling RS, Gelber R, Kiselev P, Scott G, O'Sullivan MJ, VanDyke R, Bey M, Shearer W, Jacobson RL, Jimenez E, O'Neill E, Bazin B, Delfraissy JF, Culnane M, Coombs R, Elkins M, Moye J, Stratton P, Balsley J. 1994. Reduction of maternal-infant transmission of human immunodeficiency virus type 1 with zidovudine treatment. N Engl J Med 331:1173–1180.

Darnowski JW, Goulette FA. 1994. 3′-Azido-3′-deoxythymidine cytotoxicity and metabolism in the human colon tumor cell line HCT-8. Biochem Pharmacol 48:1797–1805.

Diwan BA, Riggs CW, Logsdon D, Haines DC, Olivero OA, Rice JM, Yuspa SH, Poirier MC, Anderson LM. 1999. Multiorgan transplacental and neonatal carcinogenicity of 3′-azido-3′-deoxythymidine in mice. Toxicol Appl Pharmacol 161:82–99.

Gonzales-Cid M, Larripa I. 1994. Genotoxicity of azidothymidine (AZT) in in vitro systems. Mutat Res 321:113–118.

Helleday T. 2003. Pathways for mitotic homologous recombination in mammalian cells. Mutat Res 532:103–115.

Honma M. 2005. Generation of loss of heterozygosity and its dependency on p53 status in human lymphoblastoid cells. Environ Mol Mutagen 45:162–176.

Honma M, Zhang LS, Hayashi M, Takeshita K, Nakagawa Y, Tanaka N, Sofuni T. 1997. Illegitimate recombination leading to allelic loss and unbalanced translocation in p53-mutated human lymphoblastoid cells. Mol Cell Biol 17:4774–4781.

Honma M, Momose M, Tanabe H, Sakamoto H, Yu Y, Little JB, Sofuni T, Hayashi M. 2000. Requirement of wild-type p53 protein for maintenance of chromosomal integrity. Mol Carcinog 28:203–214.

Honma M, Momose M, Sakamoto H, Sofuni T, Hayashi M. 2001. Spindle poisons induce allelic loss in mouse lymphoma cells through mitotic non-disjunction. Mutat Res 493:101–114.

Honma M, Izumi M, Sakuraba M, Tadokoro S, Sakamoto H, Wang W, Yatagai F, Hayashi M. 2003. Deletion, rearrangement, and gene conversion; genetic consequences of chromosomal double-strand breaks in human cells. Environ Mol Mutagen 42:288–298.

Hozier J, Sawyer J, Moore M, Howard B, Clive D. 1981. Cytogenetic analysis of the L5178Y/$Tk^{+/-}$ → $Tk^{-/-}$ mouse lymphoma mutagenesis assay system. Mutat Res 84:169–181.

Jackson SP. 2002. Sensing and repairing DNA double-strand breaks. Carcinogenesis 23:687–696.

Joseph G, Grist S, Firgaira F, Turner D, Morley A. 1993. Classification of mutations at the HLA-A locus by use of the polymerase chain reaction. Environ Mol Mutagen 22:152–156.

Kennedy I, Williams S. 2000. Occupational exposure to HIV, post-exposure prophylaxis in healthcare workers. Occup Med 50:387–391.

Khanna KK, Jackson SP. 2001. DNA double-strand breaks: Signaling, repair and the cancer connection. Nat Genet 27:247–254.

Lasko D, Cavenee W. 1991. Loss of constitutional heterozygosity in human cancer. Annu Rev Genet 25:281–314.

Liber HL, Yandell DW, Little JB. 1989. A comparison of mutation induction at the Tk and Hprt loci in human lymphoblastoid cells; quantitative differences are due to an additional class of mutations at the autosomal Tk locus. Mutat Res 216:9–17.

Liechty MC, Crosby H Jr, Murthy A, Davis LM, Caspary WJ, Hozier JC. 1996. Identification of a heteromorphic microsatellite within the thymidine kinase gene in L5178Y mouse lymphoma cells. Mutat Res 371:265–271.

Meng Q, Su T, Olivero OA, Poirier MC, Shi X, Ding X, Walker VE. 2000a. Relationships between DNA incorporation, mutant frequency, and loss of heterozygosity at the TK locus in human lymphoblastoid cells exposed to 3′-Azido-3′-deoxythymidine. Toxicol Sci 54:322–329.

Meng Q, Grosovsky AJ, Shi X, Walker VE. 2000b. Mutagenicity and loss of heterozygosity at the APRT locus in human lymphoblastoid cells exposed to 3′-azido-3′-deoxythymidine. Mutagen 15:405–410.

Meng Q, Su T, O'Neill JP, Walker VE. 2002. Molecular analysis of mutations at the HPRT and TK loci of human lymphoblastoid cells after combined treatments with 3′-azido-3′-deoxythymidine and 2′,3′-dideoxyinosinedagger. Environ Mol Mutagen 39:282–295.

Mittelstaedt RA, Von Tungeln LS, Shaddock JG, Dobrovolsky VN, Beland FA, Heflich RH. 2004. Analysis of mutations in the *Tk* gene of $Tk^{(+/-)}$ mice treated as neonates with 3′-azido-3′-deoxythymidine (AZT). Mutat Res 547:63–69.

Moore MM, Clive D, Hozier JC, Howard BE, Batson AG, Turner NT, Sawyer J. 1985. Analysis of trifluorothymidine-resistant (TFTr) mutants of L5178Y/$TK^{+/-}$ mouse lymphoma cells. Mutat Res 151:161–174.

Moore MM, Harrington-Brock K, Doerr CL, Dearfield KL. 1989. Differential mutant quantitation at the mouse lymphoma Tk and CHO Hgprt loci. Mutagen 4:394–403.

Moore MM, Honma M, Clements J, Bolcsfoldi G, Burlinson B, Cifone M, Clarke J, Delongchamp R, Durward R, Fellows M, Gollapudi B, Hou S, Jenkinson P, Lloyd M, Majeska J, Myhr B, O'Donovan M, Omori T, Riach C, San R, Stankowski LF Jr, Thakur AK, Van Goethem F, Wakuri S, Yoshimura I. 2006. Mouse lymphoma thymidine kinase gene mutation assay: Follow-up meeting of the International Workshop on Genotoxicity Testing–Aberdeen, Scotland, 2003–Assay acceptance criteria, positive controls, and data evaluation. Environ Mol Mutagen 47:1–5.

NIH. 2004. Public Health Service Task Force Recommendations for Use of Antiretroviral Drugs in Pregnant HIV-1-Infected Women for Maternal Health and Interventions to Reduce Perinatal HIV-1 Transmission in the United States. Also available at http://aidsinfo.nih.gov/guidelines/

Olivero OA, Beland F A, Poirier MC. 1994. Immunofluroscent localization and quantitiation of 3′-azido-3′-deoxythymidine (AZT) incorporated into chromosomal DNA of human, hamster, and mouse cell lines. Int J Oncol 4:449–454.

Olivero OA, Anderson LM, Diwan BA, Haines DC, Harbaugh SW, Moskal TJ, Jones AB, Rice JM, Riggs CW, Logsdon D, Yuspa SH, Poirier MC. 1997. Transplancental effects of 3′-azido-2′,3′-dideoxythymidine(AZT): Tumorigenicity in mice and genotoxicity in mice and monkeys. J Natl Cancer Inst 89:1602–1608.

Olivero OA, Shearer GM, Chougnet CA, Kovacs AA, Landay AL, Baker R, Stek AM, Khoury MM, Proia LA, Kessler HA, Sha BE, Tarone RE,

Poirier MC. 1999. Incorporation of zidovudine into leukocyte DNA from HIV-1-positive adults and pregnant women, and cord blood from infants exposed in utero. AIDS 13:919–925.

Pastink A, Eeken JC, Lohman PH. 2001. Genomic integrity and the repair of double-strand DNA breaks. Mutat Res 481:37–50.

Poirier MC, Patterson TA, Slikker W Jr, Olivero OA. 1999. Incorporation of 3′-azido-3′-deoxythymidine (AZT) into fetal DNA, fetal tissue distribution of drug after infusion of pregnant late-term rhesus macaques with a human-equivalent AZT dose. J Acquir Immune Defic Syndr 22:477–483.

Ponomareva ON, Rose JA, Lasarev M, Rasey J, Turker MS. 2002. Tissue-specific deletion and discontinuous loss of heterozygosity are signatures for the mutagenic effects of ionizing radiation in solid tissues. Cancer Res 62:1518–1523.

Rathmell WK, Chu G. 1998. Mechanisms for DNA double-strand break repair in eukaryotes. In: Nickoloff JA, Hoekstra MF, editors. DNA Damage and Repair, Vol. 2. Totowa, NJ: Humana press. pp. 299–316.

Sargent RG, Brenneman MA, Wilson JH. 1997. Repair of site-specific double-strand breaks in a mammalian chromosome by homologous and illegitimate recombination. Mol Cell Biol 17:267–277.

Sawyer JR, Binz RL, Wang J, Moore MM. 2005. Multicolor spectral karyotyping of the L5178Y/Tk$^{+/-}$ 3.7.2C mouse lymphoma cell line. Environ Mol Mutatgen 47:127–131.

Storer RD, Kraynak AR, McKelvey TW, Elia MC, Goodrow TL, DeLuca JG. 1997. The mouse lymphoma L5178Y Tk$^{+/-}$ cell line is heterozygous for a codon 170 mutation in the *p53* tumor suppressor gene. Mutat Res 373:157–165.

Sussman HE, Olivero OA, Meng Q, Pietras SM, Poirier MC, O'Neill JP, Finette BA, Bauer MJ, Walker VE. 1999. Genotoxicity of 3′-azido-3′-dideoxythymidine in the human lymphoblastoid cell line, TK6: Relationships between DNA incorpration, mutant frequency, and spectrum of deletion mutations in HPRT. Mutat Res 429:249–259.

Thiagalingam S, Foy RL, Cheng KH, Lee HJ, Thiagalingam A, Ponte JF. 2002. Loss of heterozygosity as a predictor to map tumor suppressor genes in cancer: Molecular basis of its occurrence. Curr Opin Oncol 14:65–72.

Turker MS, Gage BM, Rose JA, Elroy D, Ponomareva ON, Stambrook PJ, Tischfield JA. 1999. A novel signature mutation for oxidative damage resembles a mutational pattern found commonly in human cancers. Cancer Res 59:1837–1839.

UNAIDS. 2005. Global summary of the HIV, AIDS epidemic in 2004. Also available at http://www.unaids.org

Vazquez-Padua MA, Starnes MC, Cheng YC. 1990. Incorporation of 3′-azido-3′-deoxythymidine into cellular DNA, its removal in a human leukemic cell line. Cancer Commun 2:55–62.

Veal GJ, Back DJ. 1995. Metabolism of Zidovudine. Gen Pharmacol 26: 1469–1475.

Von Tungeln LS, Hamilton LP, Dobrovolsky VN, Bishop ME, Shaddock JG, Heflich RH, Beland FA. 2002. Frequency of TK, Hprt lymphocyte mutants and bone marrow micronuclei in B6C3F1/TK$^{+/-}$ mice treated with zidovudine and lamivudine. Carcinogenesis 23:1427–1432.

Von Tungeln LS, Williams LD, Doerge DR, Shaddock JG, McGarrity LJ, Morris SM, Mittelstaedt RA, Heflich RH, Beland FA. 2007. Transplacental drug transfer and frequency of Tk and Hprt lymphocyte mutants and peripheral blood micronuclei in mice treated transplacentally with zidovudine and lamivudine. Environ Mol Mutagen 48:258–269.

Wijnhoven SW, Van Sloun PP, Kool HJ, Weeda G, Slater R, Lohman PH, Van Zeeland AA, Vrieling H. 1998. Carcinogen-induced loss of heterozygosity at the Aprt locus in somatic cells of the mouse. Proc Natl Acad Sci USA 95:13759–13764.

Wijnhoven SW, Kool HJ, Van Teijlingen CM, Van Zeeland AA, Vrieling H. 2001. Loss of heterozygosity in somatic cells of the mouse. An important step in cancer initiation? Mutat Res 473:23–36.

Zhang LS, Honma M, Matsuoka A, Suzuki T, Sofuni T, Hayashi M. 1996. Chromosome painting analysis of spontaneous and methyl methanesulfonate-induced trifluorothymidine-resistant L5178Y cell colonies. Mutat Res 370:181–190.

Zhu C, Johansson M, Karlsson A. 2000. Incorporation of nucleoside analogs into nuclear or mitochondrial DNA is determined by the intracellular phosphorylation site. J Biol Chem 275:26727–26731.

DNA REPAIR 6 (2007) 781–788

available at www.sciencedirect.com

ScienceDirect

journal homepage: www.elsevier.com/locate/dnarepair

Non-homologous end-joining for repairing I-SceI-induced DNA double strand breaks in human cells

Masamitsu Honma, Mayumi Sakuraba, Tomoko Koizumi, Yoshio Takashima, Hiroko Sakamoto, Makoto Hayashi*

Division of Genetics and Mutagenesis, National Institute of Health Sciences, 1-18-1 Kamiyoga, Setagaya-ku, Tokyo 158-8501, Japan

ARTICLE INFO

Article history:
Received 12 July 2006
Received in revised form
4 December 2006
Accepted 4 January 2007
Published on line 12 February 2007

Keywords:
DNA double strand break (DSB)
Non-homologous end-joining (NHEJ)
Homologous recombination (HR)
I-SceI
Deletion
Genomic integrity

ABSTRACT

DNA double strand breaks (DSBs) are usually repaired through either non-homologous end-joining (NHEJ) or homologous recombination (HR). While HR is basically error-free repair, NHEJ is a mutagenic pathway that leads to deletion. NHEJ must be precisely regulated to maintain genomic integrity. To clarify the role of NHEJ, we investigated the genetic consequences of NHEJ repair of DSBs in human cells. Human lymphoblastoid cell lines TSCE5 and TSCE105 have, respectively, single and double I-SceI endonuclease sites in the endogenous thymidine kinase gene (*TK*) located on chromosome 17q. I-SceI expression generated DSBs at the *TK* gene. We used the novel transfection system (Amaxa Nucleofector) to introduce an I-SceI expression vector into the cells and randomly isolated clones. We found mutations involved in the DSBs in the *TK* gene in 3% of TSCE5 cells and 30% of TSCE105 cell clones. Most of the mutations in TSCE5 were small (1–30 bp) deletions with a 0–4 bp microhomology at the junction. The others consisted of large (>60) bp deletions, an insertion, and a rearrangement. Mutants resulting from interallelic HR also occurred, but infrequently. Most of the mutations in TSCE105, on the other hand, were deletions that encompassed the two I-SceI sites generated by NHEJ at DSBs. The sequence joint was similar to that found in TSCE5 mutants. Interestingly, some mutants formed a new I-SceI site by perfectly joining the two original I-SceI sites without deletion of the broken-ends. These results support the idea that NHEJ for repairing I-SceI-induced DSBs mainly results in small or no deletions. Thus, NHEJ must help maintain genomic integrity in mammalian cells by repairing DSBs as well as by preventing many deleterious alterations.

1. Introduction

DNA double strand breaks (DSBs) are the most dangerous form of DNA damage. They can be caused by ionizing radiation (IR) or radiometric chemicals, and they can occur spontaneously during DNA replication. Other DNA damage, such as single strand breaks, easily convert to DSBs when a replication fork encounters them [1,2]. The non- or misrepair of DSBs can cause cell death or neoplastic transformation [3,4], so the accurate repair of DSBs is important for maintaining genomic integrity [5]. DSBs are generally repaired through non-homologous end-joining (NHEJ) or homologous recombination (HR) [6,7]. NHEJ joins sequences at the broken ends, which have little or no homology, in a non-conservative manner, and some genetic information is lost. HR, on the other hand, requires extensive tracts of sequence homology and is

* *Corresponding author.* Tel.: +81 3 3700 9847; fax: +81 3 3700 2348.
E-mail address: honma@nihs.go.jp (M. Honma).
1568-7864/$ – see front matter © 2007 Elsevier B.V. All rights reserved.
doi:10.1016/j.dnarep.2007.01.004

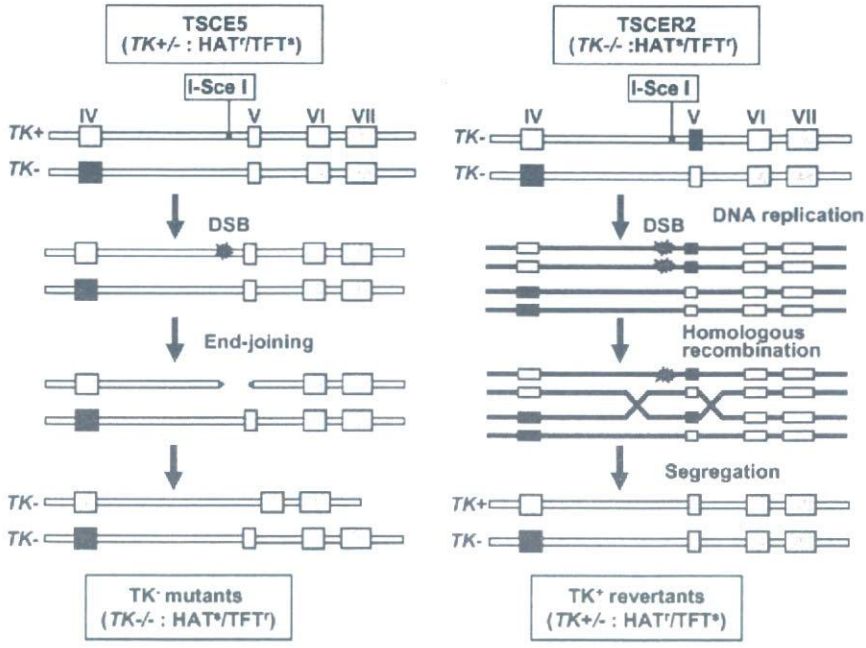

Fig. 1 – Schematic representation of the experimental system. Shadowed and closed rectangles represent the wild type and mutant exons of the *TK* gene, respectively. In TSCE5 cells, when a DSB at the I-*Sce*I site is repaired by NHEJ and causes an exon 5 deletion, TK-deficient mutants are selected in TFT medium. In TSCER2 cells, when a DSB at the I-*Sce*I site is repaired by HR, TK-proficient revertants are selected in HAT medium.

basically error-free [8]. HR is the primary DSB repair pathway in yeast and prokaryotes, but NHEJ is believed to be the primary pathway in mammalian cells [9]. HR is preferable to NHEJ because it is error-free, but NHEJ may have a different way to maintain genomic integrity.

We previously developed a human cell system to trace the fate of a DSB occurring in an endogenous single copy gene (Fig. 1) [10]. The human lymphoblastoid cell line, TSCE5, is heterozygous (+/−) and TSCER2 is compound heterozygous (−/−) for the thymidine kinase gene (*TK*), and both have an I-*Sce*I endonuclease site in intron 4. DSBs can be generated at the I-*Sce*I site by the introduction of an I-SceI enzyme expression vector. When DSBs occur at the *TK* locus, NHEJ in TSCE5 cells produces TK-deficient mutants, while HR between the alleles produces TK-proficient revertants in TSCER2 cells. Positive–negative drug selection for the TK phenotypes permits the distinction between NHEJ and HR repair mechanisms. Using the same system, we previously found that almost all I-SceI-induced DSBs in human cells are repaired by NHEJ and result in mainly 100–4000 bp deletions [10]. Drug selection, however, does not recover cells with genetic changes that are too small to influence TK function, and the resulting spectrum of mutations and reversions may be biased quantitatively as well as qualitatively.

To better understand the fate of DSBs in human cells, we randomly isolated non-selected clones after introducing DSBs and directly analyzed their DNA. A novel transfection system (Amaxa Nucleofector™) can introduce the I-SceI expression vector into most of cell population [11] and efficiently produces DSBs at the *TK* gene. With this improved method, we were able to detect cells with deletions at DSBs without drug selection and to trace the fate of DSBs without bias. We also developed a new cell line that has two I-*Sce*I sites in the *TK* gene and can be used as a model for clustering DSBs. DNA sequence analysis of the mutants in this strain revealed that both single and double DSBs were repaired predominantly by NHEJ, producing only small genetic changes, or none. We discuss how NHEJ maintains genomic integrity.

2. Materials and methods

2.1. *Human cell lines for detecting NHEJ and HR induced by a single DSB*

Human lymphoblastoid cell lines TSCE5 and TSCER2 were previously created from TK6 cells [10], which are heterozygous for a point mutation in exon 4 of the *TK* gene (*TK*+/−) (Fig. 1). TSCE5 has a 31bp DNA flagment containing the 18 bp I-*Sce*I site inserted 75bp upstream of exon 4 of the *TK*+ allele and retains TK function. TSCER2 is a TK-deficient mutant spontaneously arising from TSCE5. It has a point mutation (G:A transition) at 23bp of exon 5 of the *TK*+ allele of TSCE5. TSCER2 is compound heterozygote (*TK*−/−) for the *TK* gene. NHEJ for a DSB occurring at the I-*Sce*I site results in TK-deficient mutants in TSCE5 cells, while HR between the alleles produces TK-proficient revertants in TSCER2 cells.

2.2. *I-SceI expression and isolation of mutant clones*

We introduced the I-SceI expression vector (pCBASce) by suspending 5 × 10^6 cells in 0.1 ml Nucleofector solution V (Amaxa

Biosystem, Koeln, Germany) with 50 μg of uncut pCBASce vector (or without the vector as a control), following the manufacturer's recommendations. We then plated the cells into 96-microwell plates at 1 cell/well. Two weeks later, we randomly isolated single colonies and independently expanded them for DNA analysis.

We maintained the cell culture for 3 days and then seeded them into 96-microwell plates in the presence of 2.0 μg/ml trifluorothymidine (TFT) for isolating TK-deficient mutants or HAT (200 μM hypoxanthine, 0.1 μM aminopterin, 17.5 μM thymidine) for isolating TK-proficient revertants. We counted the drug-resistant colonies 2 or 3 weeks later [12] and calculated the mutation and revertant frequencies according to the Poisson distribution [13].

2.3. *Creating a cell line containing two I-SceI sites*

The targeting vector, pTK10, which we had used to make TSCE5 cells, consists of about 6 kb of the original *TK* gene encompassing exons 5, 6, and 7 and an I-SceI site in intron 4 [10]. We constructed pTK13 by inserting an additional 21 bp DNA fragment containing the 18 bp I-SceI sequence into pTK10 at the Nco I site in intron 5 (152 bp down stream of exon 5) using site-directed mutagenesis (GeneTailer, Invitrogen) (Fig. 4a). To obtain TK-revertant clones with two I-SceI sites in the *TK* gene, we transfected TSCER2 cells (5×10^6) with 20 μg of linearized pTK13 vector using the Nucleofector system. After 72 h, we seeded the cells into 96-microwell plates containing HAT. We identified one revertant clone, TSCE105, as correctly targeted and confirmed its molecular structure by DNA sequencing.

2.4. *DNA analysis*

To analyze mutations in the isolated TSCE5 and TSCE105 clones, we amplified the part of the *TK* gene containing the I-SceI sites by PCR, labeling forward primers with a fluorescent dye. We used the following primers for the I-SceI site in intron 4: forward (166F), 5′-TGG GAG AAT TAA GAG TTA CTC C-3′; reverse (196R), 5′-AGC TTC CAC CCC AGC AGC AGC T-3′. We used the following for the I-SceI site in intron 5: forward (251F), 5′-GGA TGG GCA CAG AGA CAC CA-3′; reverse (241R), 5′-CTG ATT CAC AAG CAC TGA AG-3′. For TSCE105 clones, we used 166F and 241R to amplify the regions containing both I-SceI sites. Amplification was performed by denaturation at 96 °C for 5 min, followed by 25 cycles of 96 °C for 30 s, 57 °C for 30 s, 72 °C for 30 s, and extension at 72 °C for 10 min. We analyzed the PCR products using an Agilent 2100 Bioanalyzer (Agilent Technologies, Waldbronn, Germany) and sequenced them with an ABI 310 genetic analyzer (Applied Biosystems, Foster City, CA).

3. Results and discussions

3.1. *Efficiency of the system for detecting NHEJ and HR repair of chromosomal DSBs using Amaxa nucleofection*

The lymphoblastoid cell lines, TSCE5 and TSCER2, which we previously developed, can trace the genetic consequences of chromosomal DSBs in the human genome. NHEJ for a DSB occurring at the I-SceI site results in TK-deficient mutants in TSCE5 cells, while HR between the alleles produces TK-proficient revertants in TSCER2 cells (Fig. 1) [10]. To introduce the I-SceI expression vector into the cells, we now used the Amaxa nucleofection system. The Amaxa Nucleofector™ can directly transfer DNA into the nucleus of the cells at high efficiency. It was designed for primary cells and hard-to-transfected cell lines such as the human B-cell lymphoblastoid [11,14]. Twenty-four hours after the nucleofection, approximately 65% of the transfected TSCE5 cells expressed the I-SceI enzyme, suggesting that DSBs were efficiently introduced into the cells (data not shown; Takashima et al., under submission).

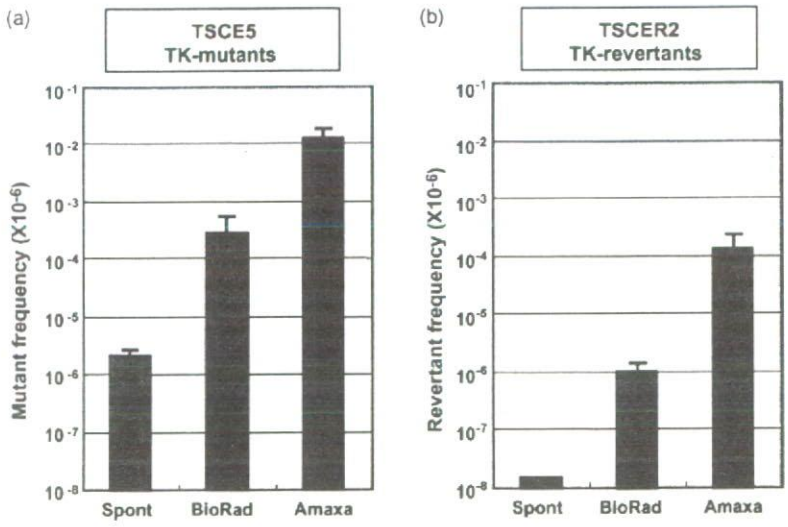

Fig. 2 – Detection of NHEJ and HR repaired DSBs using Amaxa nucleofection or BioRad electroporation. (a) Transfection of TSCE5 with the I-SceI expression vector using Amaxa nucleofection increased the TK-deficient mutant frequency more than 40-fold compared with BioRad electroporation. (b) Transfection of TSCER2 with the I-SceI expression vector using Amaxa nucleofection increased the TK-proficient revertant frequency more than 100-fold compared with BioRad electroporation.

Following Amaxa nucleofection, the mean TK mutant frequency in TSCE5 cells was 1.21%, which was more than 40-fold higher than the frequency we observed with the transfection system we had used previously (BioRad electroporation) (Fig. 2a), and the mean TK-proficient revertant frequency in TSCER2 cells was 1.22×10^{-4}, which was more than 100-fold higher than we observed previously (Fig. 2b). These results demonstrate that the Amaxa nucleofection system effciently introduced the expression vector and generated DSBs with high efficiency in the TSCE5 and TSCER2 cell lines. The relative contribution of NHEJ and HR for reparing the DSBs was 100:1. The value may be biased, however, because the drug selection assay recovers certain classes of NHEJ and HR.

3.2. *Genetic consequences of a chromosomal DSB in non-selected clones*

Because the I-*Sce*I site is inserted into intron 4 of the functional *TK* allele 75 bp upstream of exon 5, any small deletions caused by NHEJ that do not affect TK function will not be recovered as TFT-resistant mutants in the TSCE5 assay. Similarly, in the TSCER2 assay, short tract gene conversion events that do not extend to exon 5 will not be recovered as TK revertants. Thus, recovery of TK mutants and revertants by drug selection may be biased. Because nucleofection can efficiently generate DSBs at the I-*Sce*I site, however, the system enables detection of deletions and recombination in the *TK* gene without drug selection. We randomly isolated 926 transfected clones without TFT selection and directly analyzed DNAs from them. We observed that 29 (3.13%) of them had an I-*Sce*I mutation; these were usually small (<60 bp) deletions, insertions, or rearrangements (Table 1). Fig. 3 shows the DNA sequences of 21 mutants with small genetic changes. Three of them (1659, 1841, and 1893) contained a 1 bp deletion at a CCC tract within the I-*Sce*I site. Others had mostly 0–4 bp microhomologies at the junction, suggesting that the NHEJ machinery was involved. The mutant that had a 1 bp insertion at a TT tract within the I-*Sce*I site (2018) might have been generated by misalignment of the cohesive ends. The mutant that exhibited a complicated DNA rearrangement involving a 50 bp deletion combined with a 9 bp inverted sequence that was a part of deleted sequence (1614) was probably the result of sister chromatid fusion and breakage after DNA replication, as described previously [10]. Five of the mutants showed large deletions (17.2%). This fraction may correspond to the *TK* mutants in the drug selection assay. The large deletions which were commonly detected in the drug selection assay ranged from 1070 to 4030 bp, and had 4–7 bp microhomology at their junctions (data not shown) [10].

One mutant was the product of gene conversion between homologous alleles. It had lost the I-*Sce*I site and retained

Table 1 – Analysis of non-selected TSCE5 clones after I-SceI expression

Total clones	Mutant clones	Mutants (%)
926	29 (Total)	3.13
	23 (Small deletion, insertion, rearrangement; <60 bp)	2.48 (79.3)
	5 (Large deletion; >60 bp)	0.54 (17.2)
	1 (Gene conversion)	0.11 (3.4)

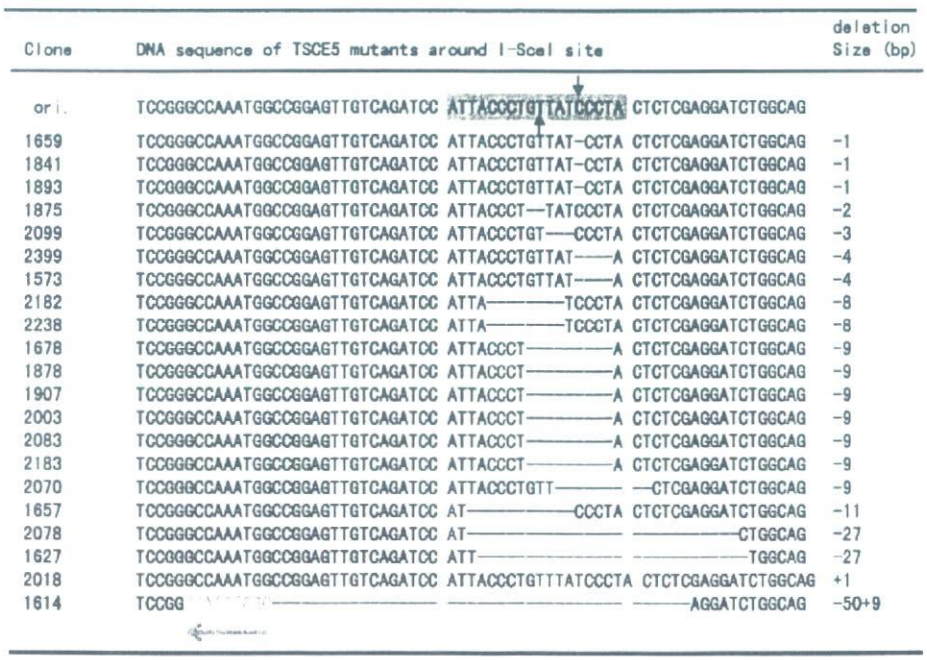

Fig. 3 – DNA sequences at the repair junction of 21 of the 26 non-selected I-SceI mutants with small (<60 bp) genetic changes in TSCE5 cells ("ori." is original sequence). The I-SceI recognition site is highlighted in orange. Arrows indicate I-SceI cleavage sites. The 1 bp deletion in the CCC tract is shown in blue and the 1 bp insertion in the TT tract is shown in green. Microhomologous sequences at junctions are shown in red. The sequence in yellow with a left arrow indicates an inverted sequence from part of a deleted sequence. (For interpretation of the references to color in this figure legend, the reader is referred to the web version of the article.)

intron 4 of the *TK* gene that had been originally connected to the I-*Sce*I site. The appearance of HR mutants was infrequent in the non-biased assay, too, suggesting that I-SceI-induced DSBs are mainly repaired by NHEJ, resulting in small deletions [10,15–17]. This does not mean that HR rarely works for DSBs, however, because our I-SceI system does not cover all HR events.

Most I-SceI systems have been developed using artificial reporter substrates based on exogenous drug-resistance or fluorescence genes and are biased in favor of detecting certain classes of deletions and recombination events [18–20]. In the present system, however, we conducted a survey of DSBs occurring in the endogenous single-copy gene, and investigated the consequences of the DSB without selection bias. We first demonstrated the mutational spectrum induced by I-SceI endonuclease in the human genome. However, it does not necessarily reflect the fate of DSBs occurring spontaneously or induced by irradiation, because our I-SceI system does not monitor sister chromatid HR, which must be the major HR pathway in mammalian cells. Other I-SceI systems setting up two tandem copies of the selective gene on the same chromosome can not also evaluate sister chromatid HR quantitatively, because both chromatids are theoretically cleaved during S/G2 phase. We may underestimate the contribution of HR in the I-SceI system.

Although the I-SceI expression vector was introduced into about 65% of the cells, the frequency of mutants at the I-*Sce*I site in the non-selection assay was still only 3.1%. Three possibilities could explain this: (1) only a small proportion of TSCE5 cells expressing the I-SceI vector may undergo a DSB, (2) most cells with DSBs may undergo apoptosis, and (3) some DSBs may go back to their original sequence by perfect joining. The last possibility would be important to the maintenance of genomic integrity following DSB repair, but its demonstration would be difficult because it is impossible to distinguish between non-cleaved and perfectly repaired I-*Sce*I sites.

3.3. *Genetic consequences of two closely separated DSBs*

To efficiently generate DSBs in the genome, we developed a cell line containing two I-*Sce*I sites in the *TK* gene. We constructed a targeting vector, pTK13, consisting of 6kb of original *TK* gene including exon 5, 6, 7 and two I-*Sce*I sites flank-

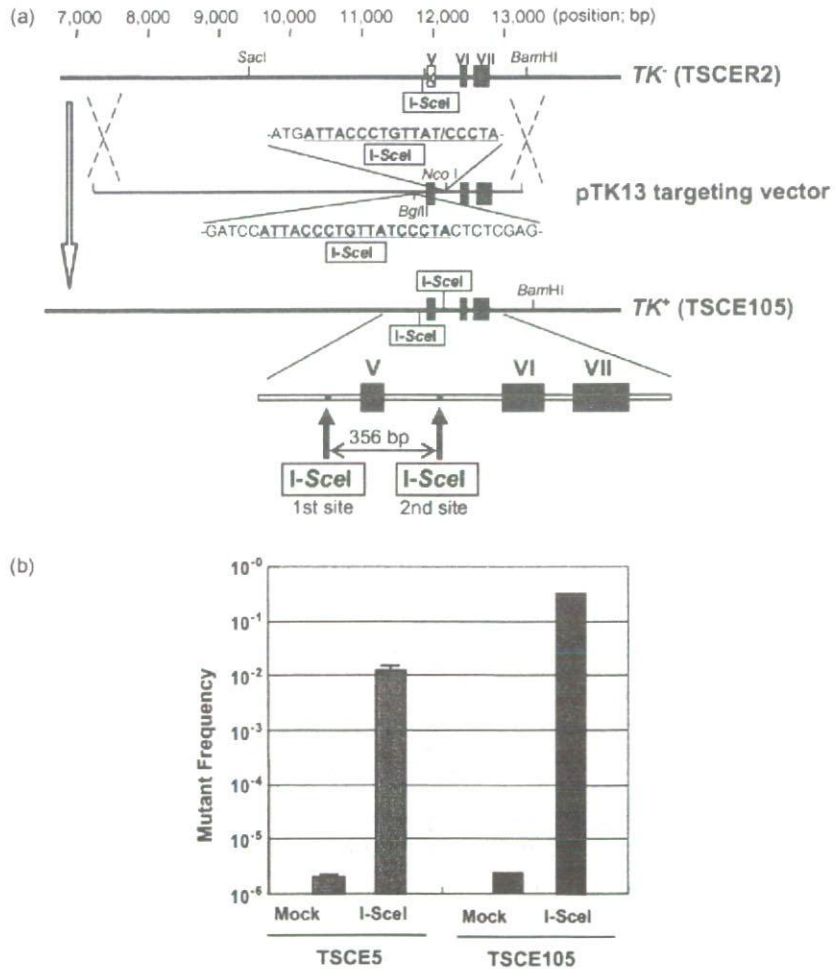

Fig. 4 – (a) Creating the TSCE105 cell line with two I-*Sce*I sites. The functional *TK* allele in the TSCE105 cell line has two I-*Sce*I recognition sites flanking exon 5, 356 bp apart. (b) The TK-deficient mutant frequency in the TSCE105 cells after introduction of DSBs by Amaxa nucleofection. The mutant frequency was 30-fold higher in TSCE105 than in TSCE5.

Table 2 – Analysis of TSCE105 mutants after I-SceI expression

Total Mutants	Type of Mutation	356bp (1st 2nd)	Number of Mutants(%)
125	Only 1st I-SceI		1 (0.8)
	Only 2nd I-SceI		47 (38)
	Both, independent		6 (4.8)
	Both, combined		70 (56)
	Perfect joining		4
	Joining with small deletion (<60bp)		31
	Joining with large deletion (>60bp)		29
	Joining with rearrangement		6
	Recombination		1 (0.8)

ing exon 5, and transfected it to TSCER2 cells (Fig. 4a). One HAT-resistant recombinant, TSCE105, had another I-*Sce*I site at intron 5 of the *TK* gene in addtion to the original I-*Sce*I site in TSCE5. The two I-*Sce*I sites are 356 bp apart, flanking exon 5 (Fig. 4a). TSCE105 was also a *TK* heterozygote and was TFT-sensitive. When we nucleofected the I-SceI expressing vector into TSCE105, the TK-deficient mutant frequency by the TFT selection assay, surprisingly, was extremely high (31.3%) (Fig. 4b). We also examined non-selectecd clones after nucleofection. Among 283 non-selected clones, 83 (29.3%) of them had a deletion mutation involving one or both I-*Sce*I sites. This mutation frequency was about the same as the TK-deficient mutation frequency in the TFT selection assay, suggesting that most mutations in TSCE105 were deletions involving coding sequence of the *TK* gene.

To investigate the genetic changes induced by the two DSBs, we analyzed 125 mutants (42 TFT-selected and 83 non-selected) and classified them into 4 types depending on whether they occurred (1) only at the first I-*Sce*I site, (2) only at the second I-*Sce*I site, (3) independenly at both I-*Sce*I sites, or (4) at the combined first and second I-*Sce*I sites (Table 2). The majority (56%) were the last type. Interestingly, four of them joined the two I-*Sce*I sites perfectly, creating a new I-*Sce*I site. Fig. 5 shows the DNA sequences around the joint sites of 26 of the 31 mutants that had small deletions. Almost all of them had a 0–4 bp microhomology at the junction, and the sequences were similar to those found around single DSB repair sites (Fig. 3).

While a single DSB in TSCE5 cells caused predominantly small deletions, two closely occuring DSBs in TSCE105 cells were not repaired independently and caused large deletions involving the two I-*Sce*I sites, indicating that multiple DSBs enhance genetic changes qualitatively as well as quantitatively. Mammalian cells may have difficulty retaining small DNA fragments generated by multiple DSBs. High doses of ionizing irradiation, too, not only increase mutation frequency but also change the mutation type to predominantly large deletions [21,22]. The genomic changes observed in TSCE5 and TSCE105 may reflect a dosage-effect, bringing about different numbers of DSBs. In both cases, however, NHEJ is involved and injury is minimized.

The mutants with perfect joining were generated by NHEJ without exonuclease processing in which the cleaved two flanking I-*Sce*I ends simply join. Most of I-SceI-induced DSBs in TSCE5 and TSCE105 cells may be perfectly joined and create a new I-*Sce*I site. Because the I-SceI enzyme is continuously expressed for at least 48 h after nucleofection (Takashima et al., under submission), the new I-*Sce*I sites generated by perfect joining are cleaved again and again. When the DSBs are occasionally joined after exonuclease processing, they accumulate as deletional mutations and are not cleaved any more (Fig. 6). Thus, the perfect joining by NHEJ is important for repairing DSBs, at least endonuclease-induced DSBs. The perfect joining by NHEJ was also reported in other I-SceI-induced DSB systems [23,24]. Van Heemst et al. demonstrated that a blunt DSB induced by the *E. coli* transposon Tn5 were repaired without loss of nucleotides in Chinese hamster cell lines, suggesting that compatible ends precisely join without deletions [25]. The efficiency or accuracy of precise NHEJ was reduced in Ku80, DNA-PK, XRCC4, or p53 deficient cells [23–26].

NHEJ in mammalian cells involves seven components—Ku70, Ku80, DNA-PKcs, Artemis, XRCC4, Cernunnos/XLF, and Ligase IV [4,7,27–29]. Although the exact role of these proteins remains unknown, three steps have been suggested: (1) end-binding, (2) terminal processing, and (3) ligation [9]. Karanjawala et al demonstrated that defects in Artemis and DNA-PKcs, which are key components in step 2 and possess substantial nucleolytic activity, do not cause severe phenotypes or genomic instability [30]. On the other hand, deficiency of Ku (step 1) or Ligase IV (step 3) confers severe radiosensitivity or lethality [30]. Thus, the second step may not be essential in NHEJ of DSBs, especially of endonuclease-induced DSBs, because the cleaved DNA ends are ligatable

Clone	DNA sequence of TSCE105 mutants around junction site	Deletion Size (bp)
	1st site 2nd site	
perfect	TCCGGGCCAAATGGCCGGAGTTGTCAGATCC ATTACCCTGTTATCCCTA GGTCTGTGCAGACTGC	
2412	TCCGGGCCAAATGGCCGGAGTTGTCAGATCC ATTACCCTGTTATCCCTA GGTCTGTGCAAACTGC	−356 (0)
2429	TCCGGGCCAAATGGCCGGAGTTGTCAGATCC ATTACCCTGTTATCCCTA GGTCTGTGCAAACTGC	−356 (0)
2445	TCCGGGCCAAATGGCCGGAGTTGTCAGATCC ATTACCCTGTTATCCCTA GGTCTGTGCAAACTGC	−356 (0)
2465	TCCGGGCCAAATGGCCGGAGTTGTCAGATCC ATTACCCTGTTATCCCTA GGTCTGTGCAAACTGC	−356 (0)
2703	TCCGGGCCAAATGGCCGGAGTTGTCAGATCC ATTACCCTGTTAT-CCTA GGTCTGTGCAAACTGC	−357 (−1)
2650	TCCGGGCCAAATGGCCGGAGTTGTCAGATCC ATTACCCTGT---CCCTA GGTCTGTGCAAACTGC	−359 (−3)
2393	TCCGGGCCAAATGGCCGGAGTTGTCAGATCC ATTACCCTG----CCCTA GGTCTGTGCAAACTGC	−360 (−4)
2453	TCCGGGCCAAATGGCCGGAGTTGTCAGATCC ATTA--------TCCCTA GGTCTGTGCAAACTGC	−364 (−8)
2434	TCCGGGCCAAATGGCCGGAGTTGTCAGATCC AT----------ATCCCTA GGTCTGTGCAAACTGC	−365 (−9)
2345	TCCGGGCCAAATGGCCGGAGTTGTCAGATCC ATTACCCT----------A GGTCTCTGCAAACGGC	−365 (−9)
2689	TCCGGGCCAAATGGCCGGAGTTGTCAGATCC ATTACCCT----------A GGTCTCTGCAAACGGC	−365 (−9)
2714	TCCGGGCCAAATGGCCGGAGTTGTCAGATCC ATTACCCT----------A GGTCTCTGCAAACGGC	−365 (−9)
2764	TCCGGGCCAAATGGCCGGAGTTGTCAGATCC ATTACCCT----------A GGTCTCTGCAAACGGC	−365 (−9)
2444	TCCGGGCCAAATGGCCGGAGTTGTCAGATCC ATTACCCT----------A GGTCTCTGCAAACGGC	−365 (−9)
2446	TCCGGGCCAAATGGCCGGAGTTGTCAGATCC ATTACCCT----------A GGTCTGTGCAAACTGC	−365 (−9)
2424	TCCGGGCCAAATGGCCGGAGTTGTCAGATCC ATTACCCT----------A GGTCTGTGCAAACTGC	−365 (−9)
2304	TCCGGGCCAAATGGCCGGAGTTGTCAGATCC AT----------CCCTA GGTCTGTGCAAACTGC	−367 (−11)
2442	TCCGGGCCAAATGGCCGGAGTTGTCAGATCC ATTACCCTGT---------- ----------GCAAACTGC	−372 (−16)
2443	TCCGGGCCAAATGTCCGGAGTTGTCAGATCC ----------TA GGTCTGTGCAAACTGC	−372 (−16)
2402	TCCGGGCCAAATGGCCGGAGTTGTCAGATCC ATTACCCTGTTAT---------- ----------AACTGC	−372 (−16)
2425	TCCGGGCCAAATGGCCGGAGTTGTCAGATCC ATTACCCTGTTATC---------- ----------TGC	−374 (−18)
2435	TCCGGGCCAAATGGCCGGAGTTGTCAGATCC ATTACCCTGTT---------- ----------GC	−378 (−22)
2713	TCCGGGCCAAATGGCCGGAGTTGTC---------- ----------TGTGCAAACTGC	−384 (−28)
2735	TCCGGGCCAAATGGCCGGAGTTGTCAGATCC ---------- ----------CTGC	−378 (−22)
2405	TCCGGGCCAAATGGCCG---------- ---------- ---TCTGTGCAAACCGC	−392 (−36)
2437	TCCGGGC---------- ---------- ----------AAACTGC	−409 (−53)

Fig. 5 – DNA sequences at the NHEJ repair junction around the I-SceI junction site in TSCE5 cells. "Perfect" is the DNA sequence when two I-SceI sites join perfectly and create a new I-SceI site (highlighted in orange). Sequences in black are upstream of the first I-SceI site and those in blue are downstream of the second I-SceI site. A total of 26 TSCE105 mutants with deletions combining two I-SceI sites are shown. Underlining indicates a new I-SceI recognition sequence produced by error-free NHEJ. Red indicates microhomologous sequences at junctions. (For interpretation of the references to color in this figure legend, the reader is referred to the web version of the article.)

and do not require terminal processing. Perfect joining by NHEJ probably skips the second step. Naturally occurring DSBs produced by oxidative stress, ionizing radiation, and DNA-damaging agents, however, do not have directly ligatable DNA ends and need some form of nucleolytic processing [7,9]. Their repair by NHEJ results in deletions, even if it works properly. In the present study, the size of the deletions caused by NHEJ, however, were relatively small. No recovered TSCE5 or TSCE105 mutants exhibited large deletions or translocations similar to those frequently observed

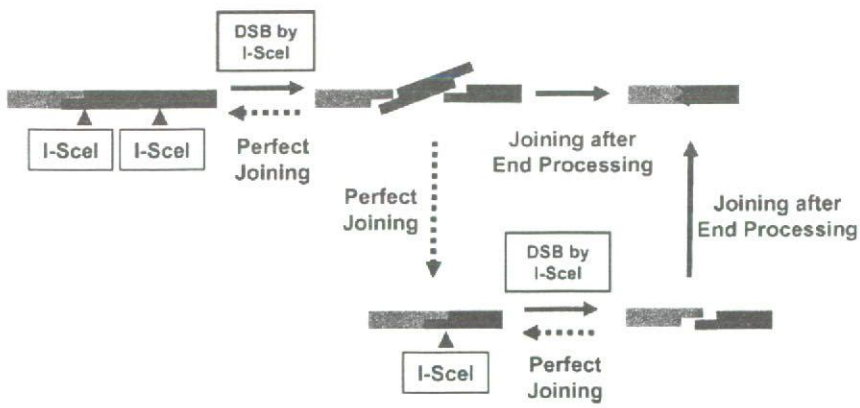

Fig. 6 – A model for NHEJ generating deletions in TSCE105 cells. When a DSB is repaired by perfect joining, an I-SceI site newly generates and is cleaved again. The rare DSB that is joined after exonuclease processing converts to a deletional mutation and accumulates in the cell population.

at the chromosome level in cancer cells [4]. This suggests that NHEJ helps maintain genomic integrity in mammalian cells by repairing DSBs as well as by preventing many deleterious alterations.

Acknowledgments

We thank Dr. Shunichi Takeda (Kyoto University) for providing the I-SceI expression vector pCBAISce. This study was supported by the Budget for Nuclear Research of the Ministry of Education, Culture, Sports, Science and Technology, based on screening and counseling by the Atomic Energy Commission.

REFERENCES

[1] K.K. Khanna, S.P. Jackson, DNA double-strand breaks: signaling, repair and the cancer connection, Nat. Genet. 27 (2001) 247–254.
[2] K.D. Mills, D.O. Ferguson, F.W. Alt, The role of DNA breaks in genomic instability and tumorigenesis, Immunol. Rev. 194 (2003) 77–95.
[3] D.C. van Gent, J.H. Hoeijmakers, R. Kanaar, Chromosomal stability and the DNA double-stranded break connection, Nat. Rev. Genet. 2 (2001) 196–206.
[4] J.H. Hoeijmakers, Genome maintenance mechanisms for preventing cancer, Nature 411 (2001) 366–374.
[5] E. Van Dyck, A.Z. Stasiak, A. Stasiak, S.C. West, Binding of double-strand breaks in DNA by human Rad52 protein, Nature 398 (1999) 728–731.
[6] S.P. Jackson, Sensing and repairing DNA double-strand breaks, Carcinogenesis 23 (2002) 687–696.
[7] K. Valerie, L.F. Povirk, Regulation and mechanisms of mammalian double-strand break repair, Oncogene 22 (2003) 5792–5812.
[8] P.A. Jeggo, DNA breakage and repair, Adv. Genet. 38 (1998) 185–218.
[9] E. Pastwa, J. Blasiak, Non-homologous DNA end joining, Acta Biochim. Pol. 50 (2003) 891–908.
[10] M. Honma, M. Izumi, M. Sakuraba, S. Tadokoro, H. Sakamoto, W. Wang, F. Yatagai, M. Hayashi, Deletion, rearrangement, and gene conversion; genetic consequences of chromosomal double-strand breaks in human cells, Environ. Mol. Mutagen. 42 (2003) 288–298.
[11] K. Maasho, A. Marusina, N.M. Reynolds, J.E. Coligan, F. Borrego, Efficient gene transfer into the human natural killer cell line, NKL, using the Amaxa nucleofection system, J. Immunol. Methods 284 (2004) 133–140.
[12] M. Honma, L.S. Zhang, M. Hayashi, K. Takeshita, Y. Nakagawa, N. Tanaka, T. Sofuni, Illegitimate recombination leading to allelic loss and unbalanced translocation in p53-mutated human lymphoblastoid cells, Mol. Cell Biol. 17 (1997) 4774–4781.
[13] E.E. Furth, W.G. Thilly, B.W. Penman, H.L. Liber, W.M. Rand, Quantitative assay for mutation in diploid human lymphoblasts using microtiter plates, Anal. Biochem. 110 (1981) 1–8.
[14] O. Gresch, F.B. Engel, D. Nesic, T.T. Tran, H.M. England, E.S. Hickman, I. Korner, L. Gan, S. Chen, S. Castro-Obregon, R. Hammermann, J. Wolf, H. Muller-Hartmann, M. Nix, G. Siebenkotten, G. Kraus, K. Lun, New non-viral method for gene transfer into primary cells, Methods 33 (2004) 151–163.
[15] J. Essers, H. van Steeg, J. de Wit, S.M. Swagemakers, M. Vermeij, J.H. Hoeijmakers, R. Kanaar, Homologous and non-homologous recombination differentially affect DNA damage repair in mice, EMBO J. 19 (2000) 1703–1710.
[16] S.P. Jackson, P.A. Jeggo, DNA double-strand break repair and V(D)J recombination: involvement of DNA-PK, Trends Biochem. Sci. 20 (1995) 412–415.
[17] J.M. Stark, M. Jasin, Extensive loss of heterozygosity is suppressed during homologous repair of chromosomal breaks, Mol. Cell Biol. 23 (2003) 733–743.
[18] P. Bertrand, D. Rouillard, A. Boulet, C. Levalois, T. Soussi, B.S. Lopez, Increase of spontaneous intrachromosomal homologous recombination in mammalian cells expressing a mutant p53 protein, Oncogene 14 (1997) 1117–1122.
[19] G.S. Boehden, N. Akyuz, K. Roemer, L. Wiesmuller, p53 mutated in the transactivation domain retains regulatory functions in homology-directed double-strand break repair, Oncogene 22 (2003) 4111–4117.
[20] C. Richardson, J.M. Stark, M. Ommundsen, M. Jasin, Rad51 overexpression promotes alternative double-strand break repair pathways and genome instability, Oncogene 23 (2004) 546–553.
[21] W.E. Bradley, A. Belouchi, K. Messing, The aprt heterozygote/hemizygote system for screening mutagenic agents allows detection of large deletions, Mutat. Res. 199 (1988) 131–138.
[22] H.L. Liber, D.W. Yandell, J.B. Little, A comparison of mutation induction at the tk and hprt loci in human lymphoblastoid cells; quantitative differences are due to an additional class of mutations at the autosomal tk locus, Mutat. Res. 216 (1989) 9–17.
[23] J. Dahm-Daphi, P. Hubbe, F. Horvath, R.A. El Awady, K.E. Bouffard, S.N. Powell, H. Willers, Nonhomologous end-joining of site-specific but not of radiation-induced DNA double-strand breaks is reduced in the presence of wild-type p53, Oncogene 24 (2005) 1663–1672.
[24] J. Guirouilh-Barbat, S. Huck, P. Bertrand, L. Pirzio, C. Desmaze, L. Sabatier, B.S. Lopez, Impact of the KU80 pathway on NHEJ-induced genome rearrangements in mammalian cells, Mol. Cell 14 (2004) 611–623.
[25] D. van Heemst, L. Brugmans, N.S. Verkaik, D.C. van Gent, End-joining of blunt DNA double-strand breaks in mammalian fibroblasts is precise and requires DNA-PK and XRCC4, DNA Rep. (Amst.) 3 (2004) 43–50.
[26] Z.E. Karanjawala, U. Grawunder, C.L. Hsieh, M.R. Lieber, The nonhomologous DNA end joining pathway is important for chromosome stability in primary fibroblasts, Curr. Biol. 9 (1999) 1501–1504.
[27] P. Ahnesorg, P. Smith, S.P. Jackson, XLF interacts with the XRCC4-DNA ligase IV complex to promote DNA nonhomologous end-joining, Cell 124 (2006) 301–313.
[28] D. Buck, L. Malivert, R. de Chasseval, A. Barraud, M.C. Fondaneche, O. Sanal, A. Plebani, J.L. Stephan, M. Hufnagel, F. le Deist, A. Fischer, A. Durandy, J.P. de Villartay, P. Revy, Cernunnos, a novel nonhomologous end-joining factor, is mutated in human immunodeficiency with microcephaly, Cell 124 (2006) 287–299.
[29] S. Burma, D.J. Chen, Role of DNA-PK in the cellular response to DNA double-strand breaks, DNA Rep. (Amst.) 3 (2004) 909–918.
[30] Z.E. Karanjawala, N. Adachi, R.A. Irvine, E.K. Oh, D. Shibata, K. Schwarz, C.L. Hsieh, M.R. Lieber, The embryonic lethality in DNA ligase IV-deficient mice is rescued by deletion of Ku: implications for unifying the heterogeneous phenotypes of NHEJ mutants, DNA Rep. (Amst.) 1 (2002) 1017–1026.

Available online at www.sciencedirect.com
ScienceDirect
ELSEVIER
Mutation Research 619 (2007) 113–123
Fundamental and Molecular Mechanisms of Mutagenesis
www.elsevier.com/locate/molmut
Community address: www.elsevier.com/locate/mutres

Potassium bromate treatment predominantly causes large deletions, but not GC > TA transversion in human cells

Yang Luan [a,b,c], Takayoshi Suzuki [a], Rajaguru Palanisamy [a,d], Yoshio Takashima [b], Hiroko Sakamoto [b], Mayumi Sakuraba [b], Tomoko Koizumi [b], Mika Saito [b,e], Hiroshi Matsufuji [e], Kazuo Yamagata [e], Teruhide Yamaguchi [a], Makoto Hayashi [b], Masamitsu Honma [b,*]

[a] *Division of Cellular and Gene Therapy Products, National Institute of Health Sciences, 1-18-1 Kamiyoga, Setagaya-ku, Tokyo 158-8501, Japan*
[b] *Division of Genetics and Mutagenesis, National Institute of Health Sciences, 1-18-1 Kamiyoga, Setagaya-ku, Tokyo 158-8501, Japan*
[c] *Center for Drug Safety Evaluation, Shanghai Institute of Materia Medica, Chinese Academy of Sciences, 294 Tai-Yuan Road, Shanghai 200031, China*
[d] *Department of Biotechnology, School of Engineering and Technology, Bharathidasan University, Palkalaiperur, Tiruchirappalli 620024, India*
[e] *Department of Food Science and Technology, College of Bioresource Sciences, Nihon University, 1866 Kameino, Fujisawa-shi, Kanagawa 252-8510, Japan*

Received 21 October 2006; received in revised form 24 February 2007; accepted 28 February 2007
Available online 4 March 2007

Abstract

Potassium bromate ($KBrO_3$) is strongly carcinogenic in rodents and mutagenic in bacteria and mammalian cells in vitro. The proposed genotoxic mechanism for $KBrO_3$ is oxidative DNA damage. $KBrO_3$ can generate high yields of 8-hydroxydeoxyguanosine (8OHdG) DNA adducts, which cause GC > TA transversions in cell-free systems. In this study, we investigated the in vitro genotoxicity of $KBrO_3$ in human lymphoblastoid TK6 cells using the comet (COM) assay, the micronucleus (MN) test, and the thymidine kinase (*TK*) gene mutation assay. After a 4 h treatment, the alkaline and neutral COM assay demonstrated that $KBrO_3$ directly yielded DNA damages including DNA double strand breaks (DSBs). $KBrO_3$ also induced MN and *TK* mutations concentration-dependently. At the highest concentration (5 mM), $KBrO_3$ induced MN and *TK* mutation frequencies that were over 30 times the background level. Molecular analysis revealed that 90% of the induced mutations were large deletions that involved loss of heterozygosity (LOH) at the *TK* locus. Ionizing-irradiation exhibited similar mutational spectrum in our system. These results indicate that the major genotoxicity of $KBrO_3$ may be due to DSBs that lead to large deletions rather than to 8OHdG adducts that lead to GC > TA transversions, as is commonly believed. To better understand the genotoxic mechanism of $KBrO_3$, we analyzed gene expression profiles of TK6 cells using Affymetrix Genechip. Some genes involved in stress, apoptosis, and DNA repair were up-regulated by the treatment of $KBrO_3$. However, we could not observe the similarity of gene expression profile in the treatment of $KBrO_3$ to ionizing-irradiation as well as oxidative damage inducers.

Keywords: Potassium bromate ($KBrO_3$); *TK*-mutation; Loss of heterozygosity (LOH); 8-Hydroxydeoxyguanosine (8OHdG); Gene expression profile

* Corresponding author. Tel.: +81 3 3700 1141x435; fax: +81 3 3700 2348.
E-mail address: honma@nihs.go.jp (M. Honma).

0027-5107/$ – see front matter © 2007 Elsevier B.V. All rights reserved.
doi:10.1016/j.mrfmmm.2007.02.029

1. Introduction

Potassium bromate ($KBrO_3$) is used as in bread making a flour improver and in the production of fish-pastes. The EU countries now prohibit its use as a food additive because of its carcinogenicity. Japan and the USA, however, permit its use in bread making on the condition that it never remains in the final product. $KBrO_3$ causes tumors, especially in kidney, in rats, and mice after long-term oral administration in drinking water [1–3]. $KBrO_3$ is also genotoxic. It is positive in in vitro genotoxicity tests – including the bacterial reverse mutation assay [1], the chromosomal aberration test conducted in Chinese hamster cells [4], and the mouse lymphoma assay [5] – and in vivo in the micronucleus test (MN) [6,7].

It has been proposed that $KBrO_3$ induces tumors through the production of oxidative damage to DNA. Oxidative DNA damage can cause mutations that contribute to the activation of oncogenes and/or the inactivation of tumor suppressor genes, thereby leading to tumorigenesis [8,9]. 8-Hydroxydeoxyguanosine (8OHdG) is the main form of oxidative DNA damage induced by $KBrO_3$ [10]. It primarily causes GC > TA transversions (as a result of the pairing of 8OHdG with A) and is believed to be responsible for mutagenesis, carcinogenesis, and aging [11,12]. $KBrO_3$ increases 8OHdG DNA adducts in vivo and in vitro [13–15]. However, $KBrO_3$ induces mutations weakly in microbial mutation assays and the *Hprt* mutation assay in mammalian cells, while it induces chromosome aberrations strongly both in vivo and in vitro [1,16,17]. These findings raise the question of whether 8OHdG is required for the mutagenic process involved in $KBrO_3$-induced carcinogenesis.

In the present study, we examined the genotoxic properties of $KBrO_3$ using the comet assay (COM), the MN test, and thymidine kinase (*TK*) gene mutation assays in human lymphoblastoid TK6 cells [18]. Unlike the X-linked hemizygous *HPRT* gene mutation assay, the *TK* mutation assay can detect not only point mutations, but also large scale chromosomal deletions, recombinations, and aneuploidy [19–21]. Most of the genetic changes observed in *TK* mutants occur in human tumors and are presumed relevant to carcinogenesis. We analyzed the *TK* mutants induced by $KBrO_3$ at the molecular level and investigated what kind of mutation predominated. We also profiled global gene expression in TK6 cell exposed to $KBrO_3$ using Affymetrix GeneChip® Expression analysis to understand the genotoxic mechanism of $KBrO_3$.

2. Materials and methods

2.1. Cell culture, chemicals, and treatment

The TK6 human lymphoblastoid cell line has been described previously [22]. Cells were maintained in RPMI 1640 medium (Gibco-BRL, Life Technology Inc., Grand Island, NY) supplemented with 10% heat-inactivated horse serum (JR Biosciences, Lenexa, KS), 200 μg/ml sodium pyruvate, 100 U/ml penicillin, and 100 μg/ml streptomycin. The cultures were incubated at 37 °C in a 5% CO_2 atmosphere with 100% humidity. $KBrO_3$ (CAS No.7758-01-2) was purchased from Wako Pure Chemical Co. (Tokyo) and dissolved in RPMI medium just before use.

We prepared 20 ml aliquots of cell suspension at a concentration of 5.0×10^5 cells/ml in 50 ml polystyrene tubes. Different concentrations of $KBrO_3$ were added to the tubes, which were then placed on a platform shaker and incubated at 37 °C for 4 h with gentle shaking. At the end of the treatment period, the cell cultures were centrifuged, washed once, and re-suspended in fresh medium. We cultured them in new flasks for the MN assay and *TK* gene mutation assay, or diluted them for plating for survival estimates.

2.2. Genotoxicity assays

After treating cells with $KBrO_3$, we prepared slides for conducting the alkaline and neutral COM assay. The alkaline COM assay was performed as previously reported [23]. For the neutral COM assay, the slide was electrophoresed with chilled neutral solution (pH 8) containing of 90 mM Tris, 2 mM Na_2EDTA, and 90 mM boric acid according to the method by Wada et al. [24]. The COM slides were stained with SYBER green (Molecular Probes, Eugene, OR) and observed by an Olympus model BX50 fluorescence microscope. At least 50 cells were captured by CCD camera, and tail length of the comet was measured. The relationship between $KBrO_3$ treatment and migration was statistically analyzed by the Dunnett test [25].

We prepared the MN test samples 48 h after treatment, as previously reported [23]. Briefly, approximately 10^6 cells suspended in hypotonic KCl solution were incubated for 10 min at room temperature, fixed twice with ice-cold methanol containing 25% acetic acid, then re-suspended in methanol containing 1% acetic acid. A drop of the suspension was placed on a clean glass slide and air-dried. The cells were stained with 40 μg/ml acridine orange solution and immediately observed with the aid of an Olympus model BX50 fluorescence microscope equipped with a U-MWBV band pass filter. At least 1000 intact interphase cells for each treatment were examined, and the cells containing MN were scored. The MN frequencies between non-treated and treated cells were statistically analyzed by Fisher's exact test [26].

We prepared the *TK* gene mutation assay samples 3 days after treatment. We seeded cells from each culture into 96-well plates at 40,000 cells/well in the presence of 3.0 μg/ml trifluo-

rothymidine (TFT). We also plated 1.6 cells/well without TFT to determine plating efficiency. All plates were incubated at 37 °C in a humidified atmosphere of 5% CO_2 in air. After 14 days, we scored colonies on the PE plates and the normal-growing (NG) *TK* mutants on the TFT plates, then re-fed the plates containing TFT with fresh TFT, incubated them for an additional 14 days, and scored them for slow-growing (SG) *TK* mutants. Mutation frequencies, relative survival (RS), and relative suspension growth (RSG) were calculated as previously described [23]. The data of mutant frequencies were statistically analyzed by Omori's method, which consists of a modified Dunnett's procedure for identifying clear negative, a Simpson–Margolin procedure for detecting downturn data, and a trend test to evaluate the dose-dependency [27].

2.3. LOH analysis of TK mutations by polymerase chain reaction (PCR)

To avoid analyzing identical mutants, we performed an additional *TK* mutation assay and isolated *TK* mutants from independent culture after a 4 h treatment with 2.5 mM $KBrO_3$. We confirmed the phenotype of the *TK* mutant clones by re-challenging them with TFT medium. We also determined the growth rate of the clones and confirmed whether they were NG or SG mutants.

Genomic DNA was extracted from the *TK* mutant cells and used as a template for PCR. We conducted the PCR-based LOH analysis of the human *TK* gene as described previously [28]. A set of primers was used to each amplify the parts of exons 4 and 7 of the *TK* gene that is heterozygous for frame shift mutations. A third primer set for amplifying parts of the β-globin was also used as the internal control. We applied quantitative-multiple PCR for co-amplification of the three regions. The PCR products were analyzed with an ABI310 genetic analyzer (PE Biosystems, Chiba, Japan), and were classified into "no LOH", "hemizygous (hemi-) LOH", or "homozygous (homo-) LOH". To determine the extent of the LOH, we analyzed 10 microsatellite loci on chromosome 17q by PCR-based LOH analysis [28]. The results were processed by GenoTyper™ software (PE Biosystems, Chiba, Japan) according to the manufacturer's guidelines.

2.4. Gene expression analysis

Total RNA was isolated from the TK6 cells after 4 h treatment with 2.5 mM $KBrO_3$ and was purified by RNeasy columns (Qiagen, Valencia, CA). We conducted a single cDNA synthesis, cRNA labeling, and cRNA fragmentation according to the manufacturer's recommendations (Affymetrix Inc., Santa Clara, CA) and employed Affymetrix GeneChip Expression analysis. The hybridization mixture for each sample was hybridized to an Affymetrix U133A human genome array. We processed the scanned data using Microarray Suite Software Version 5.0 (Affymetrix Inc., Santa Clara, CA) and imported the data into GeneSpring software (Silicon Genetics, Redwood City, CA). Signal intensity was normalized by per-gene and per-chip, and the ratios were calculated by normalizing $KBrO_3$ sample to the corresponding control sample. We used intensity-dependent (step-wise) selection of significant changes with higher cut-off value for lower signal intensity (1.75-, 2.0-, 2.25-, 2.5-, and 3.5-fold for genes intensity range of >1000, 500–1000, 100–500, 50–100, and 10–50, respectively), and up-regulated genes with a presence call in $KBrO_3$ sample, whereas down-regulated genes with a presence call in the control sample.

3. Results

3.1. Cytotoxicity and genotoxicity of $KBrO_3$

$KBrO_3$ exerted strong and concentration-dependent cytotoxicity in TK6 cells (Fig. 1). It induced approximately 50% cytotoxicity (51% RSG and 44% RS) at 2.5 mM. To investigate whether $KBrO_3$ directly causes DNA damage, we conducted the COM assay. Induction of COM tail after the treatment of in alkaline version was statistically significant 2.5 and 5 mM. In the neutral COM assay, the induction was observed form the lower concentration (Fig. 1). Because the neutral COM is thought to be associated with DNA double strand breaks (DSBs) [29], this result indicates that $KBrO_3$ directly causes DNA damage including DSBs. $KBrO_3$ also induced MN and *TK* mutation in a concentration-dependent manner and their inductions were statistically significant (Fig. 1). At the maximum concentration, it induced both MN and *TK* mutation frequencies about 30 times the control values. Two distinct phenotypic classes of *TK* mutants were generated: NG mutants grew at the same rate as the wild type (doubling time 13–17 h), and SG mutants grew at a slower rate (doubling time > 21 h). NG mutants result from intragenic mutations, while SG mutants result from gross changes (extending beyond the *TK* gene) [20]. $KBrO_3$ predominantly induced SG mutants (Fig. 1), implying that $KBrO_3$ treatment predominantly causes gross structural changes, but not small genetic alterations such as point mutations.

3.2. Molecular analysis of TK mutants

The *TK* mutants were randomly isolated from independent cultures treated with 2.5 mM $KBrO_3$ for 4 h. Table 1 shows the cytotoxicity (RSG), mutation frequency, and proportion of SG mutants induced by $KBrO_3$. We subjected 40 induced mutants to LOH analysis. Of those, 32 (80%) were SG mutants, which corresponded closely to the percentage of SG mutants induced in the assay (74.1%), indicating that the result of LOH analysis reflected the character of the induced

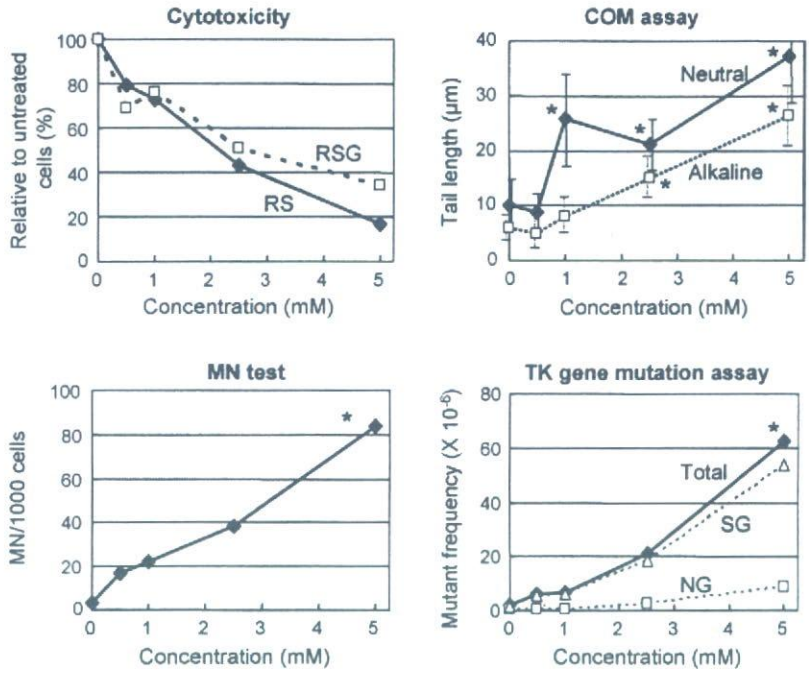

Fig. 1. Cytotoxic (relative survival, RS; relative suspension growth, RSG) and genotoxic responses (COM assay, MN test, and *TK* gene mutation assay) of TK6 cells treated with $KBrO_3$ for 4 h. Asterisk (*) statistically significant in Dunnett's test ($P < 0.05$) in COM assay, and in both pair-wise comparison and trend test ($P < 0.05$) in MN test and *TK* gene mutation assay.

mutations. Table 1 also shows the results of LOH analysis of the induced and spontaneously occurring mutants. The result of molecular analysis of spontaneous *TK* mutants was reported previously [21]. We classified the mutants into three types: non-LOH, hemizygous LOH (hemi-LOH), and homozygous LOH (homo-LOH). In general, hemi-LOH is resulted by deletion and homo-LOH is by inter-allelic homologous recombination [20]. Among the $KBrO_3$-induced mutants, 63% of NG mutants and 84% of SG mutants were hemi-LOH. In spontaneous mutants, on the other hand, majority of NG and SG mutants were non-LOH and homo-LOH, respectively. These results indicated that $KBrO_3$ predominantly induced large deletions. We previously reported the mutational spectra of *TK* mutants in TK6 cells that treated with the alkylating agent ethylmethane sulfonate (EMS), or X-irradiated [20,21]. Fig. 2 shows the comparison of the mutational spectra of spontaneous and induced *TK* mutants by EMS, X-irradiation, and $KBrO_3$. The mutation spectrum induced by $KBrO_3$ was similar to that induced by X-radiation (which also induces LOH, predominantly via deletion [21]) but not by EMS. The majority of the mutations induced by $KBrO_3$ were large deletions, but not point mutations.

Fig. 3 shows the regions of LOH and the distribution of spontaneous, X-ray-induced, and $KBrO_3$-induced

Table 1
Cytotoxic and mutational responses to $KBrO_3$, and the results of LOH analysis of normally growing (NG) and slowly growing (SG) *TK* mutants

Treatment	Cytotoxic and mutational response			LOH analysis at *TK* gene (%)			
	RSG (%)	MF ($\times 10^{-6}$)	% SG	Number	Non-LOH	Hemi-LOH	Homo-LOH
Spontaneous[a]	100	2.19	56	56			
NG mutants				19	14 (74)	3 (16)	2 (11)
SG mutants				37	0 (0)	9 (24)	28 (76)
$KBrO_3$ (2.5 mM)	51	29.4	74	39			
NG mutants				8	3 (37)	5 (63)	0 (0)
SG mutants				31	1 (3)	27 (84)	4 (13)

[a] Data from Zhan et al. [22].